Diplomarbeit

Investigations on Biological Ice Nucleation concerning Plant Materials and Structural Polysaccharides

ausgeführt am

Institut für Materialchemie

der Technischen Universität Wien

unter Anleitung von:

Ao.Univ.Prof. Dipl.-Chem. Dr.rer.nat. Hinrich Grothe

durch

Magdalena Bichler

Auhofstrasse 154/4/8, 1130 Wien

Wien am Magdalena Bichler

Danksagung

Ich möchte mich bedanken bei ….

…Prof. Hinrich Grothe für die Betreuung der Arbeit und für zahlreiche Hilfestellungen, sowie die Diskussionen im Verlauf der Arbeit

…der AG Grothe, besonders bei Laura Felgitsch, für die Unterstützung während der praktischen Arbeit und für die angenehme Arbeitsatmosphäre.

…dem Mädchenbüro vor allem für die emotionale Unterstützung und Motivation während der Endphase der Arbeit.

… und nicht zuletzt bei meiner Familie, die mich immer wieder motiviert und unterstützt hat, das Studium zu Ende zu bringen. Ganz besonders möchte ich mich bei Maxi und Tom bedanken, die mich während der letzten Monate in jeder Hinsicht unterstützt haben.

Abstract

According to Huffman et al. (2013) a burst of biological ice nuclei (IN) can be found over woodlands during and after rain events. The origin of these particles can be e.g. bacteria (e.g. *Pseudomonas syringae*), fungi (e.g. *Fusarium acuminatum* spores), and (decayed) plant litter.

B. Pummer et al. (2012) report that both pollen and pollen washing water from plants originating from the northern timberline show ice nucleation activity. These facts suggest that other parts of the plants might also act as IN due to their cold protection and cold tolerance mechanisms. Hence investigations were done concerning the ice nucleation activity of other biological materials. On the one hand, further parts of plants (mainly berries and berry juices) from the northern timberline were investigated. On the other hand, investigations were done on both water-interacting and structural polysaccharides, like pectin and chitin, as well as chemical modifications of these polysaccharides. Additionally, altering experiments were done for selected carbohydrate samples to see if treatment with ozone has any influence on the freezing properties of water. ATR-FTIR spectroscopy was done to see if the ozone treatment influences the freezing properties.

Content

1 Introduction

This chapter is mostly based on information from textbooks e.g. Seinfeld et al. (1998) and Pruppacher and Klett (1997) and references therein.

1.1 The Atmosphere

The Earth takes an exceptional position between all planets of our solar system. It lies in the so-called habitable zone, enabling the presence of liquid water. Further, it is the only planet in our solar system with an oxidising atmosphere, which facilitates life as we know it. The gaseous compounds of our atmosphere are held back by Earth's gravity. The average lifetime of a gas molecule in the atmosphere can range from a split-second to millions of years, depending on the efficiency of the removal processes.

1.1.1 Composition of the Atmosphere

The atmosphere is generally zoned in lower and upper regions, whereby the lower atmosphere is extended to the top of the stratosphere (altitude of 50km). It consists of five layers, the troposphere, the stratosphere, the mesosphere, the thermosphere and the exosphere which are divided by regions where the temperature gradient changes. These are so-called pauses. Figure 1 shows the characteristic variations of temperature and pressure within the atmosphere.

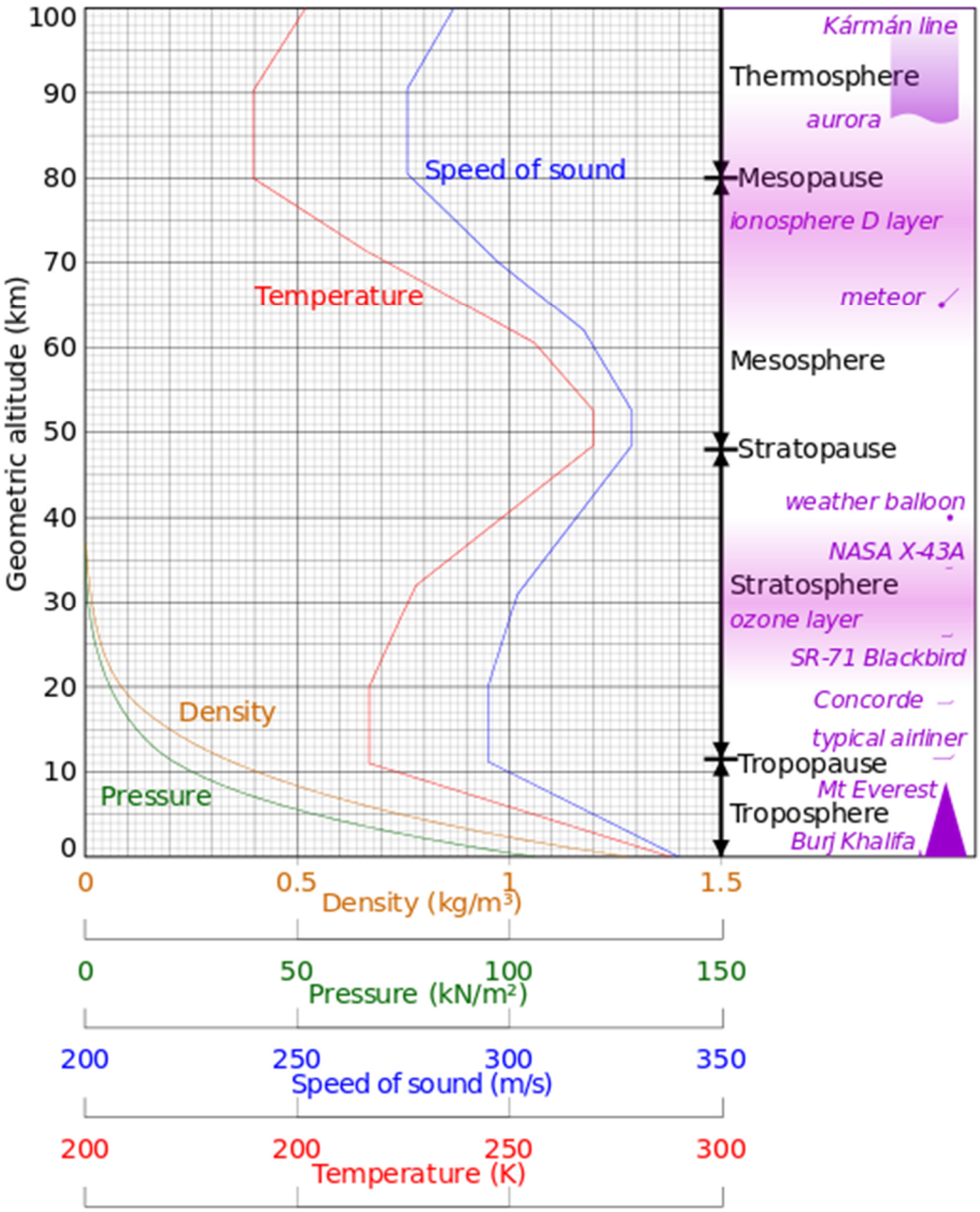

Figure 1 - layers of the Earth's Atmosphere (source: wikipedia.org)[1]

- The troposphere is the lowest layer of the atmosphere, reaching up to 10 to 15km altitude. It can be divided into the planet boundary layer (from surface up to about 1km) and the free troposphere (altitude of 1km up to the tropopause). It is characterized by decreasing temperature almost linear with height and rapid vertical mixing processes. Although the troposphere presents only a small fraction

[1] https://en.wikipedia.org/wiki/Atmosphere_of_Earth#/media/File:Comparison_US_standard_atmosphere_1962.svg (30.06.2015)

of the atmosphere's volume, it contains almost all of the atmosphere's water vapour and about 80% of the atmosphere's total mass.

- The troposphere is followed by the tropopause, which has its maximum height over the tropics and declines towards the poles.
- The stratosphere extends from the tropopause to the stratopause (45 to 55km altitude). Temperature increases with altitude. It shows vertical inhomogeneity in the chemical and radiative properties.
- The mesosphere is characterised by decreasing temperature with increasing altitude and rapid vertical mixing, followed by the mesopause, the coldest region in the atmosphere.
- The thermosphere is characterized by high temperatures since absorption of short wavelength radiation by nitrogen, oxygen and nitrogenoxides occurs. The upper part of the mesosphere and the lower thermosphere is the so called ionosphere where photoionisation processes take place.
- The exosphere is the outermost region of the atmosphere. Gas molecules with sufficient energy can escape from the Earth's gravity field (e.g. H_2 and He).

Both thermosphere and exosphere are dominated by very low pressures. Hence, present gas molecules do have high mean free paths.

Table 1- Composition of the Atmosphere

Main Components		**Trace Components**	
Nitrogen	78%	**Carbon Dioxide**	355ppm
Oxygen	21%	**Methane**	1.7ppm
Argon	1%	**Nitrous Oxide**	0,3ppm
Other Noble Gases	19,2ppm	**Carbon Oxide**	0,1ppm
Water Vapour	up to 3%		

Table 1 shows the atmospheric compounds, which are mainly nitrogen, oxygen and several noble gases, whose concentrations have remained remarkably fixed over time. The present level of oxygen is maintained by a balance between production from

photosynthesis and removal through respiration and decay of organic carbon. Atmospheric oxygen exists as diatomic O_2 and as O_3 (Ozone). The latter builds the ozone layer in the stratosphere and is responsible for its vertical structure and the temperature profile. It protects all living organisms from harmful UV radiation. In contrast, ozone generated in the lower atmosphere can have adverse effects on human health and plants. The climate is very sensitive to changes in ozone near the tropopause, since ozone is also a strong IR absorber.

Trace gases on the other hand occur in relatively small and sometimes highly variable concentrations. They comprise less than 1% and play a crucial role in the Earth's radiative balance and the properties of the atmosphere. The abundances have changed remarkably over the last two centuries. Those strong alterations (ICPP report 2013) started from the industrial revolution (1750), leading to an enormous increase of release of both particles and gases in the atmosphere, and its presence can be traced back to geological, biological, chemical, and anthropogenic processes. Greenhouse gases (CO_2, CH_4, N_2O and halogen containing compounds) act as atmospheric thermal isolators by absorbing IR radiation from the Earth's surface and reradiating a part of this radiation back to the ground. Release of the greenhouse gases has potential to lead to an increase of Earth's temperature by several degrees Celsius, which could create dramatic changes in climate and trigger extreme weather events.

Water vapour is mainly found in the lower atmosphere, since it cannot evenly surpass the low temperatures in the tropopause. Its concentration is highly variable and is controlled by variation of the vapour pressure with temperature and the abundance by evaporation and precipitation. These changes lead to feedback mechanisms like higher water vapour capacity of warm air, which results in further rising of temperature and a higher growth rate of plants due to rising CO_2-levels (limited due to the inevitable amount of N and P).

Gas molecules and aerosol particles in the atmosphere are not static. They undergo permanent alteration and are moved by circulation and a variety of transport mechanisms, both within the atmosphere's layers and throughout the pauses.

Different trace gases show large discrepancies in their spatial and temporal scales. They are divided into four groups:

- Microscale: Short-lived species remain under one hour in the atmosphere and can reach a maximum vertical distribution of 100m, e.g. NO_3, HO_2, and CH_3O_2.
- Mesoscale: Species reach a vertical distribution up to hundreds of kilometres. Their movement is driven by winds and high - and low - pressure fronts.
- Synoptic Scale: Particles are distributed over thousands of kilometres. Both mesoscale and synoptic scale species are known as moderately long-lived species, like CO, aerosols, tropospheric ozone and SO_2. They remain up to one year in the atmosphere and reach boundary layer mixing time as well as intra-hemispheric mixing time.
- Global Scale: Long-lived species stay for more than one year and mix between the hemispheres and can even reach the stratosphere. Some of these species are CH_2Br, CH_3CCl_3 and N_2O.

1.1.2 Atmospheric Aerosols

The atmosphere includes not just gases but also very diverse kinds of ambient particulate matter. Aerosols are defined as tiny particles dispersed in a gaseous phase. The common usage of aerosol just refers to the particulate components, while the gaseous phase is represented by the atmosphere. They have large impact on the climate of our planet. Some atmospheric aerosol species can reflect solar radiation back to space and act as cloud condensation nuclei showing a cooling effect. Opposed to that, black carbon has been found to further heat the atmosphere by absorbing radiation (Climate Change 2014 Synthesis Report). In addition, substances in the air can be altered by chemical and photochemical reactions and therefore do not stay stable in their properties. Removing of aerosol particles is possible by dry or wet deposition. They are larger than molecular dimensions, though the size boundary between molecular and particular structure cannot be defined precisely, starting in the nanometre scale up to thousands of micrometres.

Aerosol particles are divided into three ranges of size:

- Transient Nuclei or Aitken Nuclei Range (0.005µm - 0.1µm): They are a few percent of the total mass of airborne particles due to their small size, but they appear in high numbers. Formation of this particulate matter is enabled by condensation of hot vapours during combustion processes or by nucleation of atmospheric species directly in the atmosphere.
- Accumulation Range (0.1µm-2.5µm): Particles in this range are a substantial part of total aerosol mass and account for most of the aerosol surface area. Designation of these particles is due to their tendency to accumulation, as removal mechanisms are least efficient, resulting in longer residence times than nuclei and coarse particles. Particles are formed by coagulation of transient nuclei and by condensation of hot vapours onto existing particles.
- Mechanically Generated Aerosol Range (>2.5µm): Aerosols are formed by mechanical processes like abrasion and fracturing. These particles have both anthropogenic and natural origin. Large sedimentation velocities cause short residence times in the atmosphere.

Particles from the transient nuclei range and accumulation range are known as fine particles while mechanically generated aerosols are referred to as coarse particles. Diameter of one micrometre is a criterion for the occurrence; particles with lower diameter are found up to thousands per cm^3. Particles, which exceed this diameter, are usually found in concentration less than one particle per cm^3.

When characterizing aerosols, one must distinguish between primary and secondary aerosols. Primary aerosols arise from direct emission, whereas secondary aerosols undergo gas-to-particle conversions in the atmosphere. Secondary organic aerosols (SOAs) are an example for such species. In addition, the water of cloud droplets acts as reaction-medium, which leads to both gaseous and solid reaction products. Another criterion for characterizing aerosols is considering the origin. Aerosols of natural origin are directly emitted by natural sources. These sources can be windborne dust, sea spray or volcanoes activity. Aerosols released by anthropogenic activities are primarily combustion

products of fuels, industrial processes, nonindustrial fugitive sources (e.g. roadway dust and wind erosion of cropland) and transportation sources.

Tropospheric aerosols contain salts like sulphate, ammonium, nitrate, sodium, and chloride, trace metals, carbonaceous material, crustal elements and water. A significant fraction of these aerosols is anthropogenic in origin. Carbonaceous species can be divided into elemental and organic carbon and its mixtures. Elemental carbon consists of large, graphite-like layers, containing sp^2 hybridized C atoms. It is directly emitted through combustion processes and shows high concentrations in urban and industrial regions, posing a threat to human health. Other than that organic carbon, which shows short hydrocarbon chains, containing mostly sp^3 hybridized C atoms, a lower aromatic ratio, and a higher content in elements other than carbon and hydrogen, can be both, directly emitted and result from atmospheric condensation processes.

Aerosol particles are important factors for cloud formation, which is initiated by nucleation scavenging, which refers to activation and subsequent growth of a fraction of the aerosol population to cloud droplets. Aerosols from natural origin show high scavenging ratios from 0.5 to 1.0µm. In clouds influenced by anthropogenic sources low scavenging efficiencies are expected due to the prevalence of fine aerosol particles. During the droplet growth stage of the cloud, droplets of different sizes dilute at different rates. Small droplets grow and dilute faster than larger ones.

1.1.3 Clouds and Cloud Formation

There are several forms of atmospheric water, including clouds, fog, rain, dew and wet aerosol particles. Clouds are visible masses of liquid water droplets or ice crystals. They form and evaporate repeatedly. Due to their delivering of water as rain or snow, they are a key step in the hydrologic cycle. Approximately 60% of the Earth's surface are covered with clouds. Aside from gases and aerosols, clouds play a major climatic role by reflecting, scattering and diffracting electromagnetic radiation. High altitude clouds can cool the planet by reflecting solar radiation back to space, while low altitude heavy clouds warm the Earth by trapping energy near the surface. Besides this, clouds are a medium for

gaseous phase reactions, production of secondary species, and enabling vertical and horizontal transport of masses and heat in the atmosphere.

Clouds are categorized into four groups, low-level, midlevel, and high-level clouds, as well as clouds with vertical development. Low clouds are water clouds and consist of liquid water droplets, while mid clouds are mixed phase clouds containing both liquid water droplets and ice crystals and high clouds consist just of ice crystals. In mixed phase clouds ice and the liquid phase may be well separated in space and located in different clusters (Korolev et al., 2003). Figure 2 shows these types of clouds.

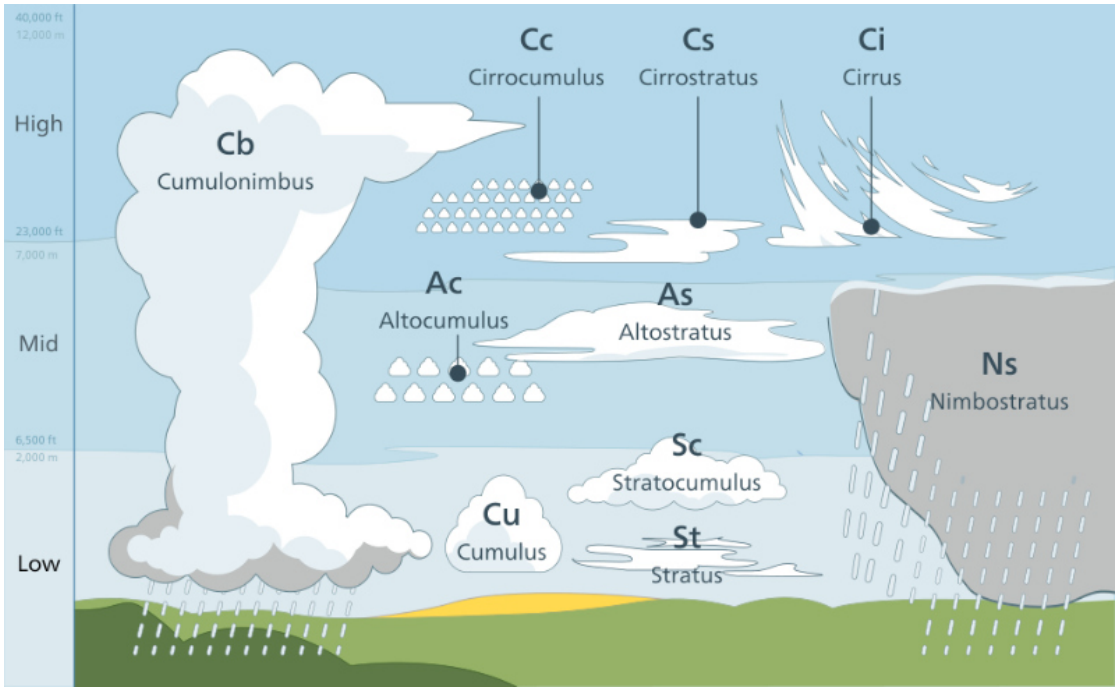

Figure 2 - clouds in the Troposphere (source: wikipedia.org)[2]

Additionally, clouds are divided into three groups due to their optical and structural properties. Stratus clouds are layers of low, often grey clouds that have little definition and do rarely produce precipitation. Their average thickness varies from 200 – 1500m. Cumulus clouds are detached and dense, rising in mounds from a level base. Cirrus clouds are high clouds with silken appearance and do usually consist of ice. Precipitating clouds

[2] https://en.wikipedia.org/wiki/Cloud#/media/File:Cloud_types_en.svg (30.06.2015)

are denoted as nimbus. Layered tropospheric clouds are generally created during the passage of a warm or cold front.

Clouds formation occurs due to supersaturation of air parcels related to water, which is caused by a substantial increase in relative humidity. It shows strong dependency on vapour pressure and temperature and is achieved by decrease of temperature of the rising air parcel. Depending on various factors, the supersaturation value has to be greater than hundred percent, in some cases even several hundred percent, which is usually a result of supercooling of moist air parcels. This process can be either isobaric or adiabatic. Isobaric conditions are present when cooling happens under constant pressure and usually is the result of either radiative loss of energy or horizontal movement of air mass over colder regions, while adiabatic conditions are achieved by ascending air parcels without any heat exchange between the rising parcel of air and the environment.

Condensation of water vapour is catalysed by so called cloud condensation nuclei (CCNs). The ability of particles to act as CCN for water droplet formation depends on their size, chemical composition and the local supersaturation. Condensation nuclei (CN) are defined as particles that form droplets at supersaturations over 400% and include all available particles. Their concentration in the atmosphere is equal to the total aerosol number concentration. On the other hand CCN represent particles that can form cloud droplets under reasonable atmospheric supersaturations and do always refer to a specific supersaturation. Their concentration corresponds in ideal systems to the concentrations of droplets. It is known that biological aerosols can also act as CCN (Möhler et al., 2007).

Water readily supercools and water clouds are frequently found in the atmosphere at sub-zero temperatures. Such clouds are quite common in the atmosphere at temperatures higher than -10°C. The likelihood of ice formation increases with decreasing temperature. At -20°C only about 10% of the clouds exist entirely of water droplets, in the majority of the clouds solid ice crystals coexist with liquid water droplets.

1.2 Ice Nucleation

At atmospheric pressure and at temperatures between 0°C and -80°C water molecules form six fold-symmetric or hexagonal ice, called ice-I_h, which is referred to in this work simply as 'ice'. X-ray diffraction studies showed that each oxygen atom is surrounded by four nearest-neighbour oxygen atoms, and these four atoms form an almost regular tetrahedron. Oxygen tetrahedrons are joined together to form a hexagonal lattice. Each water molecule is hydrogen bonded to its four nearest-neighbours. Natural ice does not behave ideally, several atomic defects can be found. Stacking faults, chemical defects, molecular vacancies (Schottky defects), interstitial molecules (Frenkel defects), ionized states and orientational defects (Bjerrum defects) are examples for derivations of ideal crystal structures. The regular oxygen tetrahedron may also arrange in cubic, diamond-type lattice. A single crystal of which however has never been found. Instead mixtures of cubic and hexagonal ices are found which can also be understood as regular series of stacking faults in a hexagonal structure (Hansen et al., 2008). These faults are particularly common in ice formed from vapour below -80°C.

When dealing with ice nucleation, one must distinguish between homogeneous and heterogeneous nucleation. Homogeneous nucleation is the term used for freezing of water without the presence of ice nuclei (IN). It depends on kinetic effects and the availability of water molecules. For small droplets, as present in clouds, it only occurs at temperatures below -38°C. In contrast, heterogeneous nucleation occurs at higher temperatures and is catalysed by so called IN.

1.2.1 Homogeneous Nucleation

In supercooled water growth of an ice embryo is a matter of molecular reorientation, involving breaking and formation of hydrogen bonds. During these kinetic processes, following a first order reaction, with constant temperature and constant pressure, a cluster of water molecules must pass from its average equilibrium position of minimum potential energy in water to a new equilibrium position in ice. The minimum size of the cluster is dependent on the temperature. Both equilibrium positions are separated by an energy barrier, the molar Gibb's free energy of activation for diffusion of water molecules

across the water-ice boundary. During nucleation process, thermodynamic does not change. Figure 3 shows the Gibb's free energy of forming a cluster, containing both surface driven and volume driven parts.

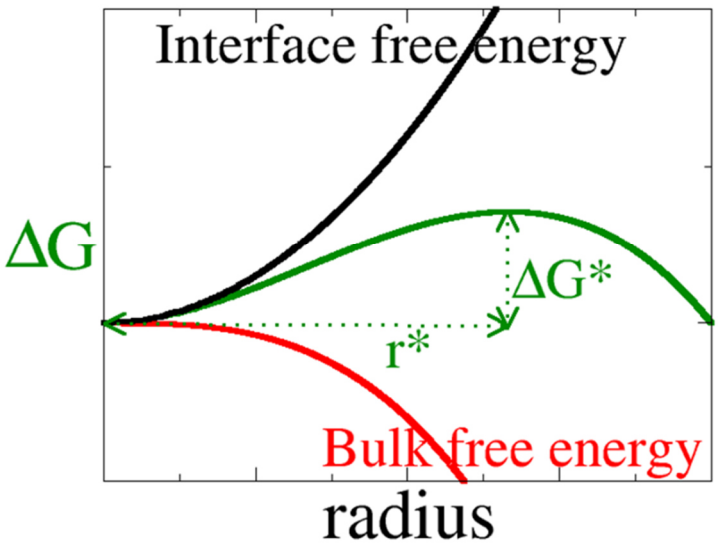

Figure 3 – Gibb's Free Energy of forming a Cluster (source: wikipedia.org)[3]

The following mathematical derivations of the Gibb's free energy and of the nucleation rates are based on a review by Murray at al., 2012 and on Murray et al., 2011.

Ice growth occurs spontaneously if a growing, ice-like water cluster passes a critical radius, as it can be seen in Figure 3. The Gibb's free energy of a cluster formation is given by Equation 1.

$$\Delta G_{cl} = \Delta G_v + \Delta G_S$$

Equation 1

ΔG_{cl} Gibb's free energy of forming a cluster

ΔG_S Gibb's energy associated with the formation an interface

3 https://en.wikipedia.org/wiki/Classical_nucleation_theory#/media/File:Plot_of_classical_nucleation_theory_prediction_for_the_free_energy_of_a_nucleus_as_a_function_of_radius.png (30.06.2015)

ΔG_v Gibb's energy associated with the bond formation between water molecules within the bulk of the cluster (negative, if saturation ratio >1)

Equation 2 gives the Gibb's free energy for a spherical cluster of radius r, containing a negative volume driven term with the third power of r and a positive surface driven term with spherical r. There, the saturation ratio, the energy of the interface and the surface tension, are decisive parameters.

$$\Delta G_{cl} = -\frac{4\pi r_i^3}{3v} kTlnS + 4\pi r_i^2 \gamma$$

Equation 2

r_i Radius of cluster, containing i molecules
k Boltzmann constant
γ Energy of interface
v Molecular volume of the condensed phase
S Saturation ratio
T Temperature

$$\frac{d\Delta G_{cl}}{dr_i} = 0$$

Equation 3

As Figure 3 shows, the Gibb's free energy curve runs through a maximum, the critical Gibb's free energy that has to be overstepped for the nucleation process. At small radii, the surface term overbalances and prohibits formation of ice crystals. Determination of critical Gibb's free energy and critical radius is achieved by determination of the zero of the first derivation, which is described by Equation 3. The Gibb's free energy of formation of the critical cluster is given by Equation 4:

$$\Delta G^* = \frac{16\pi\gamma^3 v^2}{3(kTlnS)^2}$$

Equation 4

ΔG^* Gibb's free energy of critical cluster

1.2.2 Heterogeneous Nucleation

Heterogeneous nucleation occurs at different temperatures due to the chemical and physical properties of the IN (Vali, 2014). The IN acts as catalysts and reduces the activation barrier, enabling ice nucleation at higher temperatures or at lower supersaturations. Figure 4 illustrates the effects of an IN.

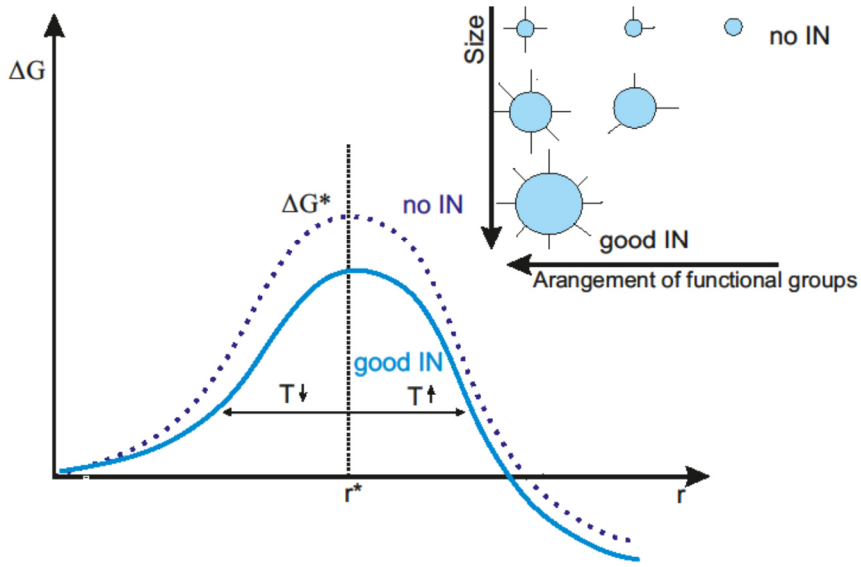

Figure 4 – catalysis of ice formation by IN

A part of the scientific community specifies IN as insoluble particles, such as mineral dust, soot, black carbon and biological materials (Lohmann and Diehl, 2006). Recent studies however show that also macromolecules are able to act as ice nucleation active substances. Pummer et al. (2012) showed that ice nucleation active macromolecules can be washed-off from birch and conifer pollen surfaces. They determined a size range of 335 – 860kDA for those macromolecules (Pummer et al., 2015). Some of them are in the same range of size as the critical cluster-size for homogeneous nucleation (see Figure 5).

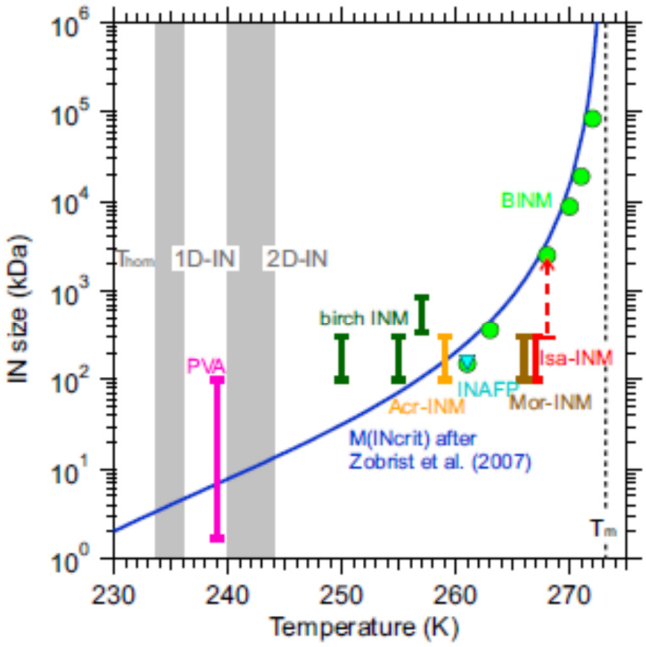

Figure 5 – Median freezing temperatures of different types of IN in reference to their size (PVA – poly vinyl alcohol, birch INM – birch ice nucleating macromolecules, Acr-INM – Acremonium implicatum ice nucleating macromolecule, INAFP – ice nucleating anti-freeze protein of Pseudomonas putida, Mor-INM – Mortierella alpina ice nucleating macromolecule, Isa-INM – Isaria farinosa ice nucleating macromolecule and BINM – bacterial ice nucleating macromolecule). The blue curve marks the critical cluster size for homogeneous nucleation (Zobrist et al. 2007) (source: Pummer et al., 2015)

Figure 5 shows the median freezing temperatures of different types of ice nuclei. The blue curve gives the critical cluster size for homogeneous nucleation, which is dependent on the temperature. The size of several IN like bacterial ice nucleating macromolecules (for further information see Chapter 1.4) is in the same range as the critical cluster size for homogeneous ice nucleation.

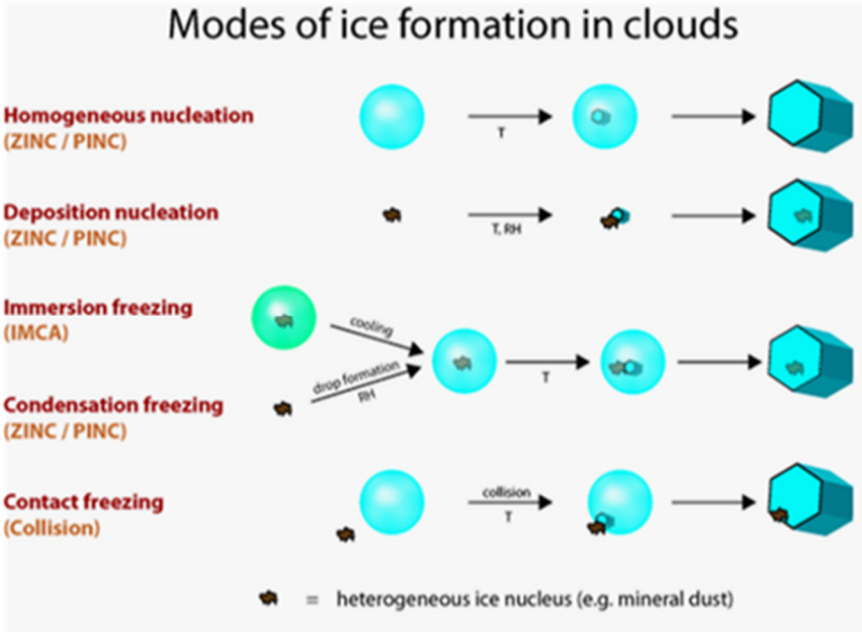

Figure 6 - modes of ice formation in clouds (source: ETH Zürich, Atmospheric and Environmental Science)

Four modes of freezing besides homogenous nucleation are known, shown in Figure 6:

- Deposition mode: Water vapour is absorbed onto the IN surface and then transformed to ice. Deposition freezing takes place at lower temperatures than the other heterogeneous freezing processes.
- Immersion freezing mode: INs are suspended into water and the freezing event occurs on the interface between IN and water. It is more prevalent at lower temperatures.
- Condensation freezing mode: INs are introduced into a supercooled droplet and freezing occurs immediately after the introduction, usually the most effective process at slight supercoolings.

  Condensation and immersion freezing are difficult to separate since the most probably way for immersing a particle inside a droplet is through condensation on that particle (Murray et al., 2011). Besides this, these two modes of freezing are the main important freezing modes in ice and mixed phase clouds.
- Contact freezing mode: Supercooled droplets collide with an IN and initiate ice formation. It is always initiated at higher temperatures than immersion freezing and is limited by the collision efficiency.

In supercooled clouds most of the heterogeneous freezing between 0°C and -35°C is initiated by contact freezing of dust, especially at higher temperatures (higher than -10°C). Immersion freezing is most important at cold temperatures below -20°C (Lohmann and Diehl, 2006). In mixed phase clouds formation of ice occurs in two stages. First vapour pressure exceeds the saturation pressure over water and liquid droplets get activated. Second droplet freezing occurs through activation of contact or immersion ice nucleators (Korolev et al., 2003). In mesosphere clouds homogeneous nucleation of crystalline ice particles directly from the vapour phase may be possible (Murray and Jensen, 2010).

1.2.3 Nucleation Rates

The **homogeneous nucleation** rate J_{hom} is the probability of nucleation events per unit of time for a population of identical ice embryos. Equation 5 gives the frozen drop fraction of an array of water droplets, dependent on total number of droplets, droplet volume, time and nucleation rate.

$$n_{hom} = n_{tot}(1 - \exp(-J_{hom}Vt)$$

Equation 5

$$ln\left(\frac{n_{tot} - n_{hom}}{n_{tot}}\right) = -J_{hom}Vt = \ln(1 - f_{ice})$$

Equation 6

$$ln\left(\frac{n_{tot} - n_{hom}}{n_{tot}}\right) = -J_{hom}V\Delta t = \ln(1 - f_{ice})$$

Equation 7

n_{hom}	Number of homogeneous frozen droplets
n_{tot}	Total number of droplets
J_{hom}	Nucleation rate in case of homogeneous freezing
V	Volume of one droplet
t	Time
f_{ice}	Fraction of frozen droplets
Δt	Temperature range for determination of J_{hom}

Due to both logarithmic calculus and summarizing the logarithms, Equation 5 is transformed into Equation 6. The term $\left(\frac{n_{tot}-n_{hom}}{n_{tot}}\right)$ can also be written as$(1 - f_{ice})$. For

determination of J_{hom} as function of time with insignificant changes in temperature, the time t may be replaced by the time interval Δt (Equation 7). These modifications allow experimental determination of the nucleation rates.

For **heterogeneous nucleation,** the nucleation rate is defined as the probability of nucleation events per unit surface area of substrate and is given by Equation 8:

$$ln\left(\frac{n_{tot} - n_i}{n_{tot}}\right) = -J_i \sigma \Delta t = \ln(1 - f_{ice})$$

Equation 8

J_i Heterogeneous nucleation rate coefficient of species i

σ Surface area

In comparison to the homogeneous nucleation rate, the volume must be substituted by the number of active sites per particle. This model supposes that freezing probability is similar for all droplets. The heterogeneous nucleation rates are dependent on the concentration of active sites in the droplet. The interactions of water with the foreign surface can be characterized in terms of the contact angle between surface and water, which is an interfacial energy. Niedermeier et al. (2011) used these contact angle distributions with consideration of stochastic and singular freezing behaviour for development of the so called soccer ball model, which allows description and modelling of heterogeneous nucleation. Here, heterogeneous nucleation is driven by two main mechanisms:

- Stochastic model of heterogeneous nucleation – time-dependent nucleation:
  Stochastic nucleation follows first order chemical kinetics and is a result of molecular fluctuations within water and ice embryo.
- Singular model of heterogeneous nucleation – temperature-dependent nucleation:
  Each nucleation site is characterized by a specific temperature due to allocation of ice nucleating particles in sub-samples and to location of active sites on the surface. Each active site has its own freezing temperature.

(Vali, 2014)

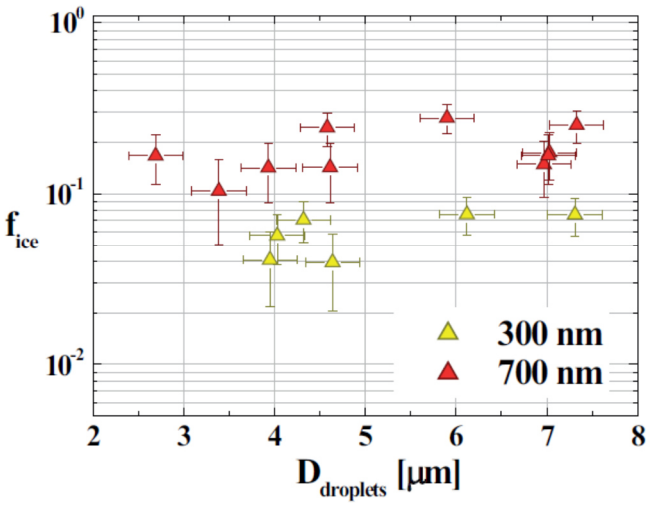

Figure 7 – ice fraction in dependence of droplet diameter for kaolinite particles with both 300nm (yellow) and 700nm (red) mobility diameter (source private communication S. Hartmann[4])

Figure 7 shows the dependency of the ice fraction on the droplet diameter. For both mobility diameters 30nm and 700 nm, the ice fraction is not dependent on the droplet diameter. Hence, there is no correlation between both droplet volume ($V = \frac{4}{3}\left(\frac{d}{2}\right)^2 \pi$) and concentration (particles per droplet volume) and the ice fraction. Deductive reasoning of these facts is the concentration independency of heterogeneous nucleation.

[4] Susan Hartmann, TROPOS Leibnitz - Institut für Troposphärenforschung

1.3 Biological Ice Nucleation

A major part of global precipitation, no matter if snow, hail or rain, has gone through some ice processes. Many materials have been found to trigger heterogeneous ice nucleation. This ability can show direct input on our atmosphere by influencing ice cloud formation. Ice clouds show a different scattering behaviour than clouds consisting of liquid droplets. Further they tend to precipitate faster. Therefore heterogeneous ice nucleation holds the ability to show direct influence on our climate (Lohmann et al., 2002, Mishchenko et al., 1996). Predicting this influence is complicated since these processes are only poorly understood.

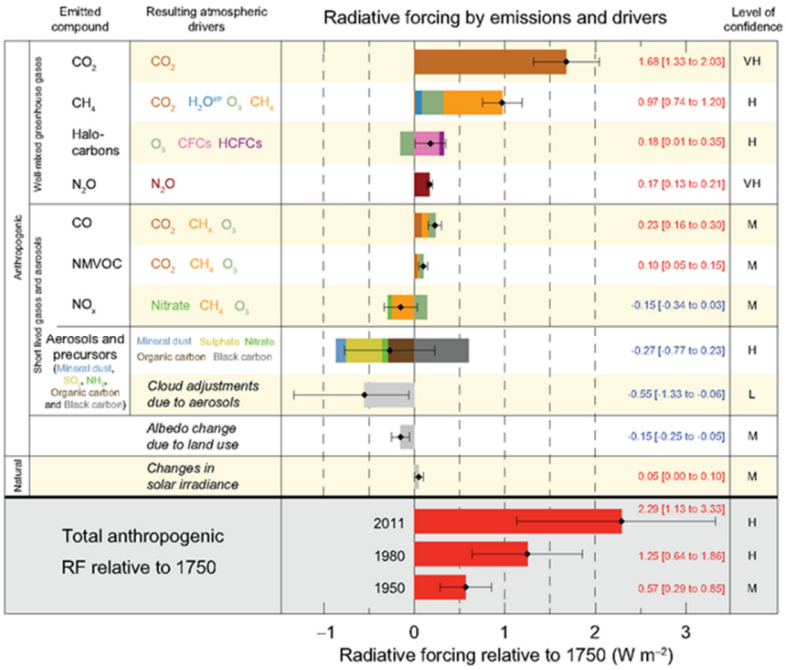

Figure 8 – radiative forcing relative to 1750 (source IPCC Report 2013)

Figure 8 shows the radiative forcing relative to 1750, which was starting point of the already mentioned industrial revolution. The highest uncertainty in regards of influencing factors concerning global warming are aerosol cloud interactions. Furthermore, this factor seems to have a cooling effect on our planet and is worth further investigations.

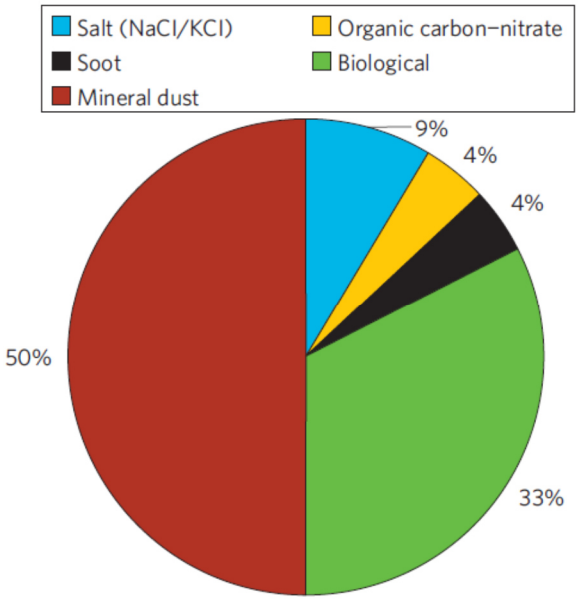

Figure 9 – contribution of particle types contained in atmospheric ice crystals (source: Pratt et al., 2009)

Atmospheric mass spectrometry on the platform of an aircraft reveals that a large fraction of ice crystal residues in high ice clouds has biological origin, including eukaryotic, prokaryotic and viral fragments (Pratt et al., 2009). Biological aerosols are large molecules and/or airborne particles with average size between 10nm and 100µm. They can either be alive, carrying living organisms or are released from living organisms (e.g. biofilms) and at least some of them act as ice nuclei (Ariya et al., 2004 and Ariya et al., 2009). In situ measurements of biological particles in ice crystals suggest terrestric origin of the biological IN (Pratt et al., 2009). Biological IN from air samples can be assigned to one of three major taxonomic groups: plant, bacteria and fungi (Bowers et al., 2009). Hence these substances have to be assigned.

Huffman et al (2013) showed during their measurement campaign in Colorado (USA) that there is an enormous burst of fluorescent biological aerosol particles in the air right after rain events over woodlands. Detection was carried out by fluorescence microscopy, based on the cellular metabolites NAD(P)H and riboflavin, which are markers for life since they are components of all living organisms (Huffman et al., 2012). These biological materials contain many different ice nuclei, whereby there is a direct correlation between the concentration of ice nuclei and the concentration of biological particles. About 1000

taxonomic units[5] of all domains of life could be identified as source of these biological particles by DNA analysis (Huffman et al., 2013).

More than forty years ago, Schnell and Vali did investigations on the ice nucleation activity of different biological materials. They found IN in decayed plant materials from different climatic zones, including tropical[6], humid mesothermal[7] and microthermal[8] zone. However, no investigations on plant materials from the arctic or subarctic zone were done, but in marine materials IN were found, without any further identifications. Investigations of atmospheric IN showed that aerosols in the humid mesothermal zone contain the highest amount of IN. Investigation of plant associated microbes resulted in the identification of the bacterium *Pseudomonas syringae* as ice nucleation active plant pathogen microbe. Fungi did not show any effects. (Schnell and Vali, 1976; Vali et al., 1976). A literature research shows that since the 1970ies meteorological investigations on biological IN were rare, but some were published by biologists (e.g. Kieft and Ruscetti, 1990; Maki et al., 1974; Kajava and Lindow, 1993; Pouleur et al., 1992). Recently, this topic was shifted into a bright focus again, and multidisciplinary investigations were started. This is important since biological IN play a crucial role in the web of precipitations. For example, biological IN were found in fresh snow samples from worldwide locations (Christener et al., 2008). However not all biological IN in soil and vegetation litter have bacterial origin (Möhler et al., 2007). David Sands was the first to introduce the concept of bioprecipitation and showed that there is an interrelationship between ice nuclei and weather (Sands et al., 1982).

[5] Group of organisms that is phylogenetically related and can be distinguished from other groups by certain properties.
[6] Region of the Earth that surrounds the equator
[7] Earth's temperate zones with moderate amount of heat and mild winters
[8] North America's and Eurasia's zones with continental climate

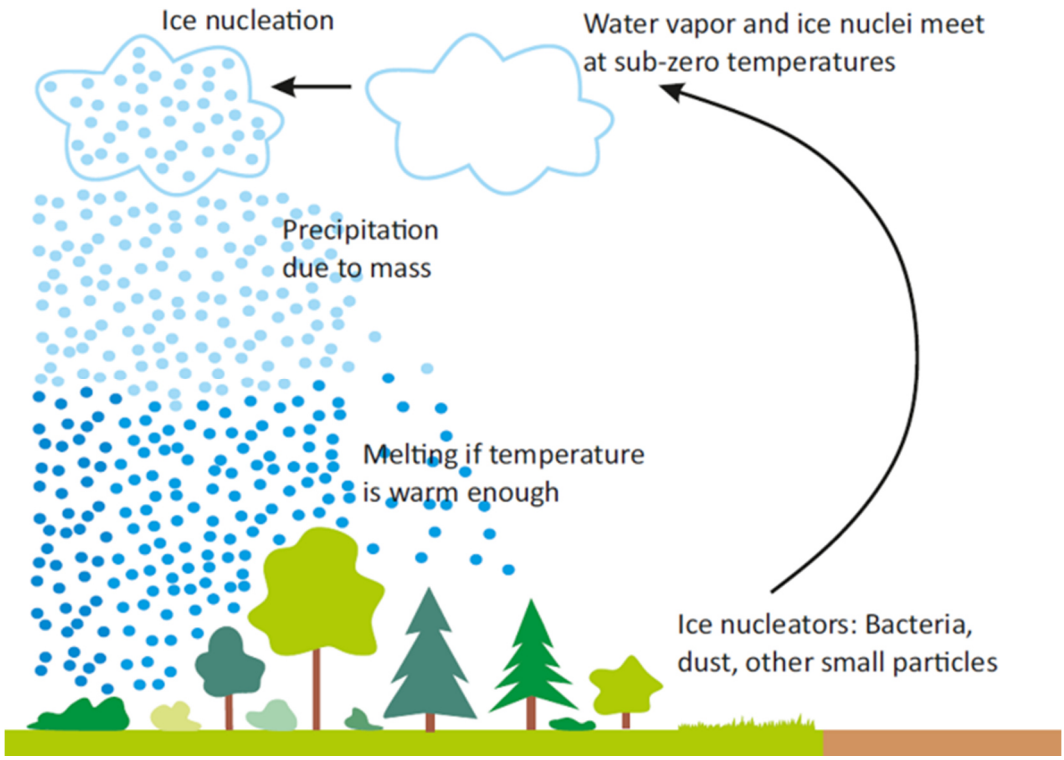

Figure 10 – concept of bioprecipitation

Figure 10 shows the concept of bioprecipitation, which means that in humid weather periods ice nucleators are released with water vapour from plants into the air and up into the atmosphere. These ice nucleators meet with water vapour at sub-zero temperatures and ice nucleation occurs and leads to precipitation, depending on the temperature as rain or snow. Biological materials must be integrated into droplets to precipitate. Rain provides more water for plants and microorganisms, plant masses increases and microorganisms (bacteria, rust fungi) benefit from both plant mass and water, leading to production of more IN and starting the positive correlating cycle again between the release of IN and more precipitation (Morris et al., 2014).

Many microorganisms are known as ice nucleating agents. Gamma-Proteobacteria are the most active prokaryotic ice nuclei generating agents, like the already mentioned *Pseudomonas syringae* and different *Xanthomonas spp.* and *Pseudoxanthomonas spp.* These species are generally present on vegetation in their natural habitats. A small number of ice nucleation active bacterial cells in a cloud is enough to induce precipitation (Joly et al., 2013). Also eukaryotic microbes are known to act as IN. The marine diatom

Thalassiosira pseudonana can act as an efficient ice nucleus under tropospheric conditions. Diatoms are widely spread over the oceans and can be released together with other marine materials by bubble bursting (Knopf et al., 2011). Lichen genera were found to show ice nucleation activity. Kieft and Ruscetti demonstrated that the fungal part of the lichen *Rhizoplaca chrysoleuca* acts as IN. Further investigations manifested a structural relationship between die IN of *Pseudomonas syringae* and the fungal partner (Kieft and Ruscetti, 1990). *Fusarium acuminatum* and *Fusarium avenaceum* show ice nucleation activity in the range of *Pseudomonas spp.* while other *Fusarium spp*. do not have the property to take influence on the freezing behaviour of water (Pouleur et al., 1992). Obviously, ice nucleation is an exceptional property and the question comes up why single species within a family show this property and why others often in the same environment do not.

We do not know much about the ice nucleation activity of non-living biological fragments. Over long time, these fragments (such as pollen, leaf litter or insects) were disregarded because of their huge aerodynamic diameter of 10 - 100µm. Only recently, a particular research interest was on tree pollen like birch. Some kinds of pollen can act as IN in deposition mode as well as in immersion mode and contact freezing mode (Diehl et al., 2001; Diehl et al., 2002). Pummer et al. (2012) report that suspendable macromolecules, which are released from pollen, are ice nucleation active. These pollen are particularly from trees living near the northern timberline (Pummer et al., 2012). Since there is arctic climate at the northern timberline (Figure 11), plants get cryo-stress. Vegetation periods are short and in winter often permafrost occurs and even during the warm season there is night frost. Plants had to develop mechanisms that protects them from climatic stress during evolution by a huge variety of different procedures.

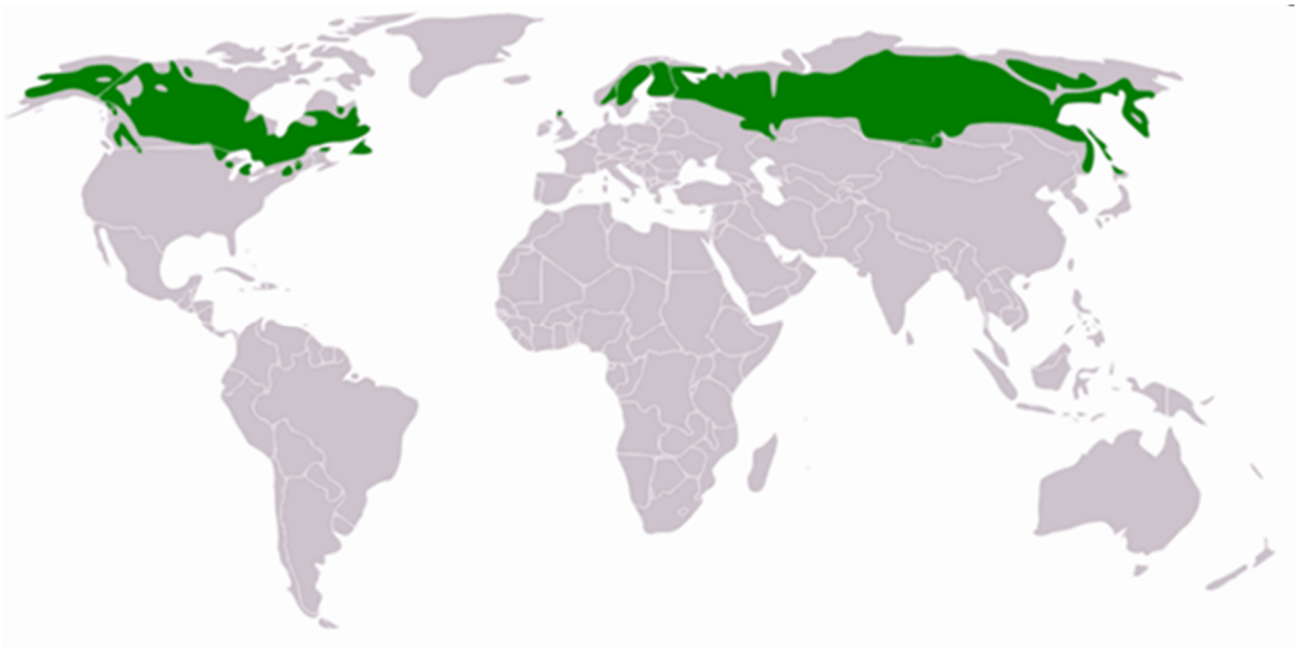

Figure 11 - northern timberline (50°N to 70°N) (source: wikipedia.org[9])

[9] https://en.wikipedia.org/wiki/Taiga#/media/File:Distribution_Taiga.png (30.6.2015)

1.4 Cold-tolerance of plants

This chapter is mostly based on information out of textbooks e.g. Lee, Warren and Gusta, Biological Ice Nucleation and its Applications, 1995, chapter 7-8, and references therein.

Frost and snow can damage plants very seriously. Frost injury is primarily caused by the formation of ice in plant tissues at temperatures below 0°C. The plasma membrane is considered the primary site of freezing injuries which manifest themselves as both mechanical damage and dehydration injury. Plants must avoid or escape ice formation to prevent these damages. Throughout evolution, several mechanisms were developed:

- Extracellular polysaccharides act as freezing inhibitors, which are dispersed in the liquid water of the extracellular space. They prevent frost damages by both binding and/or being captured in growing ice crystals as well as by forming a cohesive film at the ice-liquid interface, which decreases the crystal growth rate.
- Some plants fortify their cell wall with structural carbohydrates (e.g. sucrose) and/or glycoproteins (e.g. extensin) as response to low temperature. This augmentation allows them to isolate their cytoplasm and to increase rigidity, which might prevent the cell from collapsing due to freezing-induced dehydration.
- The composition of the plasma-membrane is also changed as response to cold temperatures. Protein and lipid components can be varied. Altering of the lipid fraction shows changes in the degree of unsaturated fatty acids, composition of sterols, increases in phospholipid to protein ratio and declines in sterol to phospholipid ratio.
- Concentration of soluble carbohydrates (e.g. sorbitol, mannitol, raffinose) in the cytoplasm is often altered due to sub-zero temperatures, which results in major changes of the total osmotic potential (freeze-induced dehydration), metabolic effects (secondary protective substances and metabolic energy), cryoprotective effects (cellular structures might be protected during freeze/thaw cycles), and glass formation effects (stopping all biochemical and most physical activities).
- Accumulations of proteins in the cytoplasm have been observed in many plants due to cold stress. Both total protein content and specific polypeptide species are increased, including structural proteins as well as enzymes. In addition, induction

of freezing tolerance occurs due to formation of proteins. Some of them have direct cryoprotective functions (eg. proteins in spinach- and cabbage leaves) and act as chaperones, guarding other proteins from denaturation. Also antifreeze proteins are known to be found in plant tissues, which exhibit sequences that are homologous to sequences of antifreeze proteins of other species.

- Some plants are known to have intrinsic IN (e.g. *Lobelia telekii*) since intracellular ice formation leads to membrane damages. Some trees are known to have extrinsic IN and are able to supercool their xylem ray parenchyma cells to -45°C.
- Timberline conifers and other wooden flora in the subalpine vegetation zone are known to have deep undercooled water in their stem tissue (Becwar et al., 1981).
- Tissue freezing might be catalysed by external ice nucleation active sites that might be associated with tracheids (elongated cells in the xylem) and xylem vessels.

A particular interest of this work lies on IN that are contained in plants from the northern timberline. Hence a particular view on both antifreeze and ice nucleating proteins is given. Both classes of protein are summarised as ice binding proteins (IBPs).

1.4.1 Antifreeze proteins

Antifreeze proteins (AFPs) have been discovered in many species, including plants, bacteria, cold tolerating insects and fishes. Davies and Sykes (1997) categorized them into antifreezing glycoproteins (AFGP) as well as in type I – IV AFPs. Different types of AFPs exhibit distinctions in their primary, secondary and tertiary structure, as well as in the ice binding planes. Also differences in both size and absorption kinetics were determined (Drori et al., 2014; Davies, 2014). Due to these differences, AFPs might have evolved independently from several different progenitors (Jia and Davies, 2002). Nevertheless all of them protect their host organisms from freezing damages in cold environments at sub-zero temperatures by causing thermal hysteresis[10]. AFPs are widely spread in many domains of life. Some of their functions are depicted in Figure 12. (A) shows the antifreezing function of AFPs in blood vessels. Due to these proteins, ice crystals are

[10] Temperature difference between the melting point (elevated) and freezing point (depressed) of an ice crystal caused by adsorption of IBPs to the ice surface (Davies 2014).

inhibited in their growth and cannot damage the organism (e.g. arctic flounder). (B) shows ice recrystallization inhibition, which occurs at high sub-zero temperatures. Presence of AFPs prevents small ice crystals from disappearing due to migration of water across the grain boundaries to larger crystals. Solutes are excluded from ice during freezing events and are present at the ice grain boundaries. They do not prevent freezing, but protect plant tissues from dehydration and structural damages through growing ice crystals. Ice binding proteins that work outside of organisms are shown in Figure 12 (C). These microorganisms live in ice-filed habitats. (C) left shows green algae that release AFPs to keep water channels open, which allows them to live in this ecological niche, including respiring, taking up nutrients and dividing. Also fungi, yeasts and bacteria have this property. Thus, these proteins have ice-structuring functions. (C) right shows marine bacteria (*Marinomas primoryensis*) that include ice binding domains on the N-terminal region of their cell wall proteins. Hence, due to these AFP domains the bacteria can attach themselves to the underside of sea or lake ice, where the obligate aerobic bacterium benefits from oxygen and nutrients that are released from photosynthetic microorganisms.

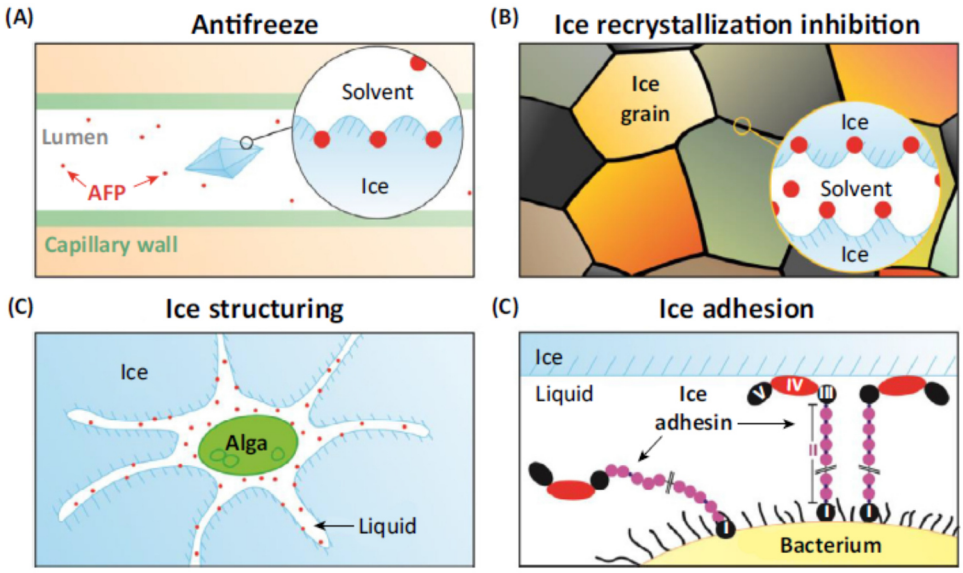

Figure 12 – roles of AFPs (source: Davies 2014)

Also several plant species produce AFPs, which are homologous to pathogenesis-related proteins (Griffith and Yaish, 2004). These plant origin proteins can protect the cells from frost damage by both antifreeze effect and inhibition of ice recrystallization.

On average, the size of these proteins is between 3 and 16kDa (Drori et al., 2014). They do not lead to a change of the melting temperature, but the freezing point is decreased. The mechanism seems to be noncolligative (Wierzbicki et al., 2007). Investigations of the ice binding domains of fish, insects and microorganisms showed high structural diversities in both primary and secondary structures of the proteins. Latter include α-helices, helix-bundles, β-solenoids and proline-helices. Wierzbicki et al. report that amino acid sequences containing Thr-Ala-Ala in helical structures of type I AFPs interact with the ice crystals. Also globular folds of mixed structures could be found. Some proteins are stabilized by cations. The IBP (ice binding protein) diversity of plants has not been investigated in detail, yet (Davies, 2014).

The effects of AFPs on water below 0°C was investigated in numerous molecular modelling studies. Two selected results of literature research are depicted to show that different types of AFPs do have similar mechanisms at the water/ice interface. Smolin and Daggett (2008) did molecular modelling of type III AFP [11] (found in blood serum of the polar fish ocean pout). Their calculations indicate that water at the ice-binding surface is more ordered in ice-like patterns than around non-ice binding parts of the protein. Differences between these two sites get more distinctive at lower temperatures. Due to these structures the ice binding site seems to have both high affinity and high specificity to ice. Hence, the ice-binding surface is primed to bind circulating ice and to inhibit it growth this way. Wierzbicki et al. (2007) identified properties for orientation of type I AFPs[12] (e.g. in winter flounder) by computational calculations. They report that there is phase equilibrium between the ice and water, and that the protein is immersed in this semisolid/semiliquid phase of the ice/water interface. Hence, the interactions between protein and ice cannot be considered as receptor-ligand interactions because the receptor cannot be clearly distinguished from the solvent. The boundary layer is about 10 -20Å wide and provides no distinctive ice surface for the protein. They suggest that the protein,

[11] Dimer with 7kDa, secondary structure: noncannonical short β strands; globular tertiary structure with some flat surfaces and unique 3D fold, ice binding plane close to 10-10 (Davies and Sykes, 1997)
[12] 3-5kDa Protein, primary structure > 60% Alanin, secondary structure: 100% α-helices, tertiary structure: single α helix, which is the longest free standing helix of AFPs, ice binding plane 20-21/21-10 (Davies and Sykes, 1997)

by interacting with the ice/water interfacial region, ‘‘poisons’’ it. Thus the ice is stopped from growing by accumulating at this interface

The ice binding sites of AFPs show high similarity to the ice nucleating sites of ice nucleating proteins. Latter are significantly longer than AFPs and size seems to be primary discriminating factor between these two kinds of proteins (Davies, 2014 and Garnham et al., 2011).

1.4.2 Ice nucleating proteins

Several biological species like bacteria, insects and plants are known to produce ice nucleation proteins (INPs). These proteins order water molecules on their surface in an ice-like pattern allowing the formation of ice crystals at higher temperatures. As mentioned above, IBPs of plants were not investigated in detail. Hence, the ice nucleation active protein of the bacterial plant pathogen *Pseudomonas syringae* that was investigated in detail is introduced to get an idea how INPs work.

The ice nucleation active protein of *Pseudomonas syringae* consists of three areas, an N-terminal unique domain, a C-terminal unique domain and a large central repeating domain, that comprises 70% of the sequence (primary structure of the protein) and is responsible for the nucleation events. Figure13 shows the 3-dimensional structure of the ice binding part of the protein, which shows amazing structural similarity to ice crystals.

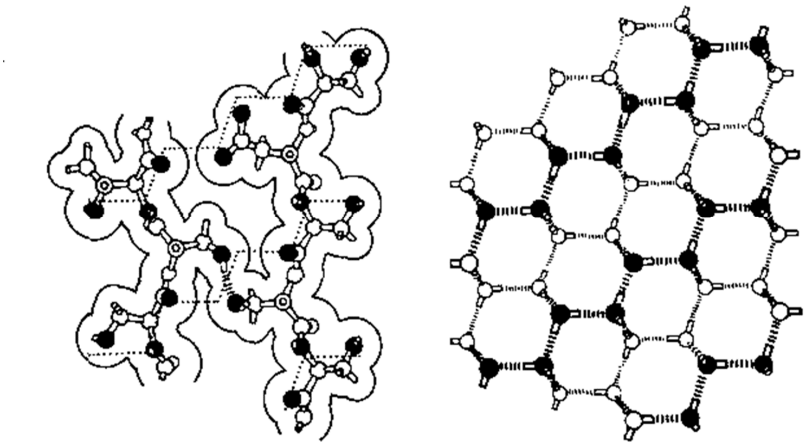

Figure 13 – structural similarity of INP and water (Kajava and Lindow, 1993)

The secondary structure of this central sequence is dominated by β-hairpins that are contacting each other by sidechains and having donors and acceptors arranged similarly to them in ice. These β-sheets are rich of serine and threonine, with extremely low proportion of amino acids with hydrophobic residues. Conformation is fixed by interpeptide hydrogen bonds, independent from amino acid composition. Additional stabilisation is given by Serine ladders. Donors and acceptors of hydrogen bonds on the ice nucleating protein are arranged complementary to them in ice. Because of the structures of repetitive elements, the hydrogen bonds to water might occur every 8^{th}, 16^{th} or 48^{th} residues. The most likely folding pattern consists of β-hairpins, having Glycine at the turns of the hairpin and highly conserved Serine and Threonine residues in the middle of the strands, which allows them to act as template for ice formation. The core contains modest hydrophobic residues.

Tertiary structure of these proteins is a flat aggregate on surfaces of membranes by interdigitating the 48 residue units, while quaternary structure contains alternating flat rectangular bands and trapezoidal bands, which allow efficient docking of the molecules and maintain an ice-like surface over the whole aggregate.
(Kajava and Lindow, 1993; Garnham et al., 2011)

2 Experimental

The focus of this work lies on IN with biological origin. As mentioned in Chapter 1.3, in-situ measurements in the upper troposphere showed that 33% of atmospheric ice crystal residues have biological origin (Pratt et al., 2009), which suggest that there might be a range of atmospheric relevant biological IN. Hence, plant materials and components of all domains of life have to be investigated concerning their ice nucleation activity.

Since it is known that pollen from the northern timberline show ice nucleation activity, (Pummer et al., 2012) plant samples with the same origin were chosen. As mentioned in Chapter 1.2, the IN of birch pollen are suspendable macromolecules (Pummer et al., 2015) and can be washed off. Therefore plant materials from the northern timberline were investigated due to their influence on the freezing properties of water. State of the art of these materials is given in the following section

2.1 State of the art

The following section gives an overview over the state of the art of plant materials from the northern timberline which are known to influence the freezing properties of water.

2.1.1 Sea Buckthorn

Sea buckthorn is widely distributed over Europe and Asia and grows under different climate types. It is known to live in Tuscany as well as at the northern timberline in Scandinavia and the Himalayas. Ripening occurs from August to December. Fruits often remain on bushes over winter if not eaten by birds and seem to tolerate freezing without obvious damages. Juice of different sea buckthorn species are known to have nucleation temperatures in the range between -6.1°C and -15.1°C, depending on their homeland.

- The wild type of *Hyppophae rhamnoides* collected in Denmark and cultures in Canada freezes between -2°C and -3°C.
- The subspecies *caucasica* seems to have two distinct populations of ice nuclei, freezing at about -7°C and at -14°C.
- Russian cultivars are active at temperatures between -7°C and -10°C.

Nevertheless no correlation between climate and freezing temperature can be declared. Hence it is not known whether IN occurs to prevent the seeds from germination or to increase the frost tolerance of plants. During ripening the content of L-ascorbic acid and flavonols significantly increases. Rapid and repeated freezing and thawing processes reduce the ice nucleation activity of sea buckthorn samples. IN temperatures increase significantly in the autumn cold which suggest that the IN are produced as response to early frost. Additionally, sea buckthorn juice seems to show freezing point depression. Also the IN might be extracted from leave tissues.
(Lundheim and Wahlberg, 1998; Jeppsson and Gao, 2000; Jann et al., 1997)

2.1.2 Blueberry

Stem, flower bud and leaves of *Vaccinium corymbosum* and *Vaccinium ashei*, older than 20 years and being domiciled in Japan are known to show intrinsic (extracellular) ice nucleation activity, developing and changing seasonally. The highest ice nucleation

activity was found in stems, followed by flower buds, fruits and leaves. Investigating the stem showed that the ice nucleation activity is not located to special stem segments, meaning that the stem can initiate freezing at any position spontaneously. There is a quantitative relationship between stem mass and ice nucleation activity, which can be assigned to the bark tissues while xylem and pith have much lower levels. Infra-red thermography shows that freezing is initiated in several positions in the stem and propagates into the leaves without any external IN. Investigations of cellular material result in recognizing the accumulation of the IN in cell walls and intercellular structural components.
(Kishimoto et al., 2014)

2.2 Sample Selection

In our temperature zone plant material from the arctic and subarctic region is difficult to access. Therefore juices and frozen berries were bought directly from companies and investigated by cryo-microscopy. The chemical components extracted from living organisms are structural polysaccharides. Further samples without chemical modifications were chitin, pectin, alginate and many others. Chemical modifications of chitin and pectin were investigated to see if any conversion processes take place, which might also occur in their natural environment. Additionally, chemical altering was done by ozone treatment of some samples to simulate oxidation processes of the atmosphere.

2.3 Sample Preparation

2.3.1 Structural Polysaccharides

The samples of structural and water-interacting polysaccharides were obtained as milled powder or as flocculation that had to be converted into smaller particles by milling with a ball mill (Retch mixer mill MM 400) under dry conditions. Chitin and chitin derivatives were provided by Dr. Verena Seidl-Seiboth, Institute of Chemical Engineering, Vienna University of Technology. Fa. C. E. Roeper GmbH allocated binding agents, while chemically modified pectins were obtained from Fa. Herbstreith & Fox Corporate Group. The apple pectin flocculation was bought in a drugstore and stored in the lab for several years. The exact denomination is "Apfel-Pektin Flocken Nahrungsergänzungsmittel Karl Minck – Apfelfaser und Apfelpektin zur ballaststoffhaltigen Nahrungsergänzung" from "Pharma Naturheilmittel". Best before date of this sample is 04/2013. All used structural polysaccharides are listed in Table 2 and Table 3.

Table 2 – used chitin and modified chitin samples

Sample	Denomination	Company	Annotations
Chitin	C7170-100G	Sigma Aldrich	Chitin from shrimp shells
Chitosan	740179-1G	Sigma-Aldrich	molecular weight: 140 000-220 000g degree of acetylation: <40 mol %
Chitin Resin	S6651S	New England Biolabs	Chitin beads (usually used as column material)
Colloidal Chitin	-	-	Prepared from chitin from shrimp shells (Seidl et al., 2005)
tri-Acetyl-Chitotriose		Megazyme	
Hexaacetyl-Chitohexaose		Megazyme	

Table 3 – used binding agents and pectin samples

Sample	Denomination	Company	Annotations
Pectin	APA 103 HM Apfelpektin	C. E. Roeper GmbH	
Alginate	NA 4012 Sodium Alginate min 400 mPas	C. E. Roeper GmbH	
Agar-Agar	8925 Q CERO Agar Agar Pulver Gracelaria min. 900 gel	C. E. Roeper GmbH	
Carob Gum	040 T CERAGUM Johannisbrot-kernmehl 2200 cps	C. E. Roeper GmbH	
Guar Gum	166 CERAMEHL Guarkernmehl min 3500 cps / 200 mesh	C. E. Roeper GmbH	
AU 015	Pektin Amid AU 015	Herbstreit & Fox Corporate Group	31% esterification 19% amidation 84% galacturonic acid
AU 202	Pektin Classic AU 202	Herbstreit & Fox Corporate Group	68% esterification 79% galacturonic acid
AU602	Pektin Classic AU 602	Herbstreit & Fox Corporate Group	49% esterification 79% galacturonic acid
AU 701	Pektin Classic AU 701	Herbstreit & Fox Corporate Group	38% esterification 80% galacturonic acid
Applepectin	Apfelpektin	Carl Minck / Pharma Naturheilmittel	Best before date: 04/2013

2.3.1.1 Solutions

For investigating the samples with cryo-microscopy, solutions had to be prepared. Saturated solutions of the carbohydrate samples in ultrapure MilliQ® water were generated. Since these saturated solutions were highly viscous, they were diluted for the experiments until they could be easily pipetted. Dissolving was supported by strongly shaking with a shaking device (Vortex-Schüttler, lab dancer, VWR collection) and by ultrasound bath (EMAG Emmi-40HC) at 70°C. For preparation of the chitin samples, some grains were suspended and dissolved in ultrapure MilliQ® water.

2.3.1.2 Altering of the Pectin Samples

For simulation of processes up in the atmosphere, chemically modified pectin samples were altered with ozone by using an Ozone Generator (Fischer Ozon Ozon-Generator 500) (Figure 14).

Figure 14 – ozone generator

Altering was performed for 10 minutes to ensure efficient treatment. Figure 15 shows the apparatus for ozone treatment. The washing flasks were filled with KI solution to prevent ozone from getting into the fume hood. The apparatus allows close contact between powdery samples and gaseous ozone for sufficient oxidation.

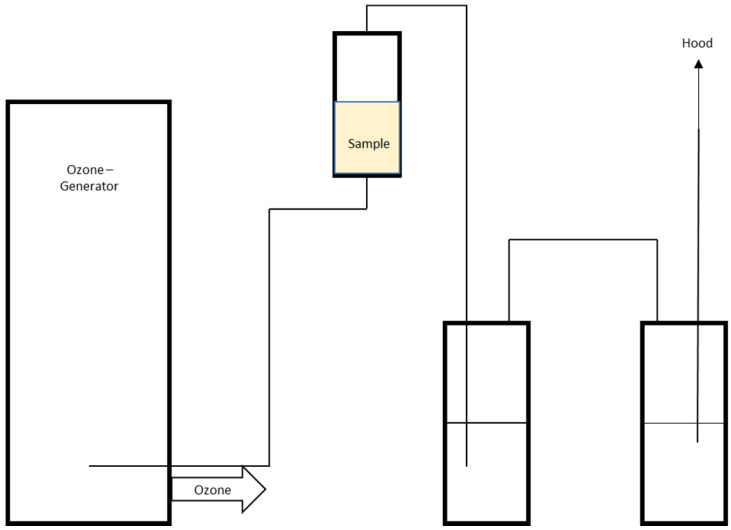

Figure 15 – construction for ozone treatment

2.3.2 Plant Materials

Fruit samples were obtained as pure juices with pasteurisation treatment or as frozen berries. The pure juices were bought from both Weleda (sea buckthorn) and Alnavit (sea buckthorn, black currant, lingonberry, cranberry, chockeberry, sambucus and blueberry) as well as elite naturel (mulberry). All samples that were obtained from “Alnavit” were marked as “Muttersaft”, meaning directly pressed berry juice without further treatment. Just mild pasteurization processes at about 60°C were done to avoid microbial spoilage. Also the “Weleda” sea buckthorn juice was marked “Muttersaft”. Frozen berries were bought from Spar Natur*pur (raspberries), Obst Oswald (rowanberries) and Polarica (cloudberries and fenberries). These frozen fruits were extracted by using a lab centrifuge (Sartorius 2-16P) or by using a household juice separator (Gastroback Smart Health Juicer Pro) to get juices for cryo-microscopy, depending on the textural quality of the fruits. All plant extracts that were used for production of extract were bought from “Sonnentor” and produced by biodynamic agriculture. Plant extracts were obtained by heating some of the dry plant materials in ultrapure MilliQ water for 30 minutes to 70°C. Small plant particles were separated by using the lab centrifuge with 3000g for 20 minutes. All necessary dilution steps were done by using ultrapure MilliQ® water. Table 4 gives an overview over the used dilution steps.

Table 4 – overview over used dilution steps

Dilution	Parts Sample	Parts Water
1:1	1	1
1:2	1	2
1:5	1	4
1:10	1	9
1:50	1	49
1:100	1	99
1:200	1	199

2.4 Methods

All biological samples were analysed by cryo-microscopy to determine their ice nucleation activity. Additional characterisation of structural polysaccharides was done by attenuated total reflection Fourier transformation infrared spectroscopy (ATR-FTIR). It was tried to develop a method for differential scanning calorimetry (DSC) in addition to cryo-microscopy for determination the T_{50}-values. The advantage of cryo-DSC would be that less experimental effort is required.

2.4.1 Differential Scanning Calorimetry Measurements

DSC is a thermo-analytical method for detecting heat changes during phase transitions. As sample containers small metal vessels (100µl) are used. As reference, an empty DSC capsule was used and heated to 500°C before the first measurements to ensure that no reactions take place during the following measurements. Throughout the measurements, sample and reference are maintained at the same temperature and are cooled or heated at defined rates. Liquid nitrogen is the refrigerant for the cooling processes.

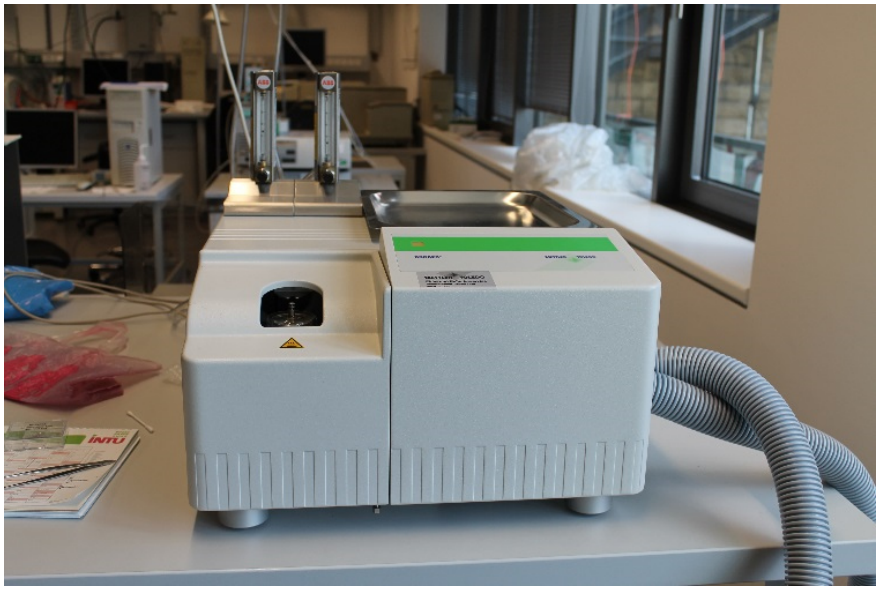

Figure 16 – Mettler Toledo DSC823^e differential scanning calorimetry - unit

If a phase transition occurs heat is either released or consumed by the sample in relation to the reference, depending on the process which is either endothermic or exothermic.

For examination of the samples, water-in-oil emulsions were generated. The samples contained always of one part water and two to four parts of the oil.

2.4.2 Cryo-Microscopy

Cryo-microscopy was used for determination of T_{50}-values (temperature where f_{ice} is 50%) and of the nucleation rates. It is based on optical light microscopy. Figure 17 shows the used reflected light microscope (Olympus BX51M), expanded with the cryo-cell and a primitive cooling system containing a water pump and water-ice blend. A blow-dryer is used to avoid fogging of the cell. The top of the microscope is connected with a digital camera and a computer to take pictures during freezing processes. The software Skope Tek minisee (version x86, 1.1.404) allows to take magnified pictures of the samples with the help of the digital camera at different temperatures.

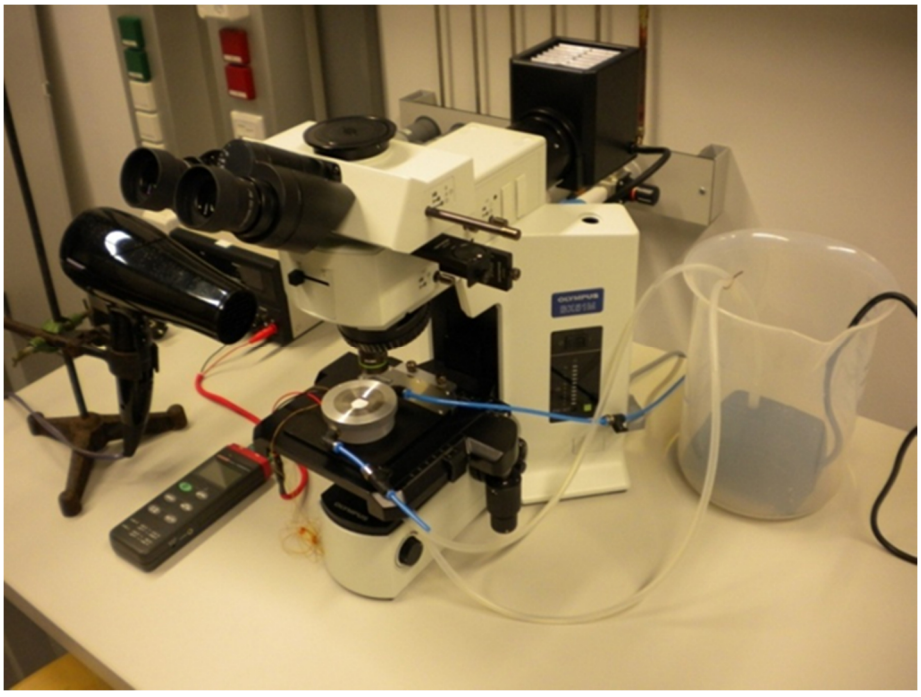

Figure 17 – Reflected light microscope with cryo-cell and cooling-system

Figure 17 gives a detailed view on the cryo-cell. It contains a thermal element (type K) for detection of temperature. The single stage Peltier-element (HighTech Peltier Element QuickCool QC-31-1.4-3.7M) and the copper cooling block, connected with the cooling system mentioned above, allow cooling down of the system during the measurements.

Applying of current forces the Peletier-element to pump heat from the surface of the element to the down side, connected with the cooling block. This effect is based on thermoelectricity effects and depends on the current rating. The amount of transported heat depends on the materials of the Peltier element (commonly both n- and p-semiconductors) and the applied current. This context is given by Equation 9.

$$\dot{Q} = (\Pi_A - \Pi_B)I$$

Equation 9

$\dot{Q}$	transported heat
Π_i	Peltier coefficient of material i
I	current

Controlling of current with a laboratory power supply allows regulating the temperature inside of the cell. The cryo-cell can be locked up airtight to avoid gas exchange when measuring. Additionally gas in- and outlet are part of the system to flush the system with nitrogen for getting rid of humidity.

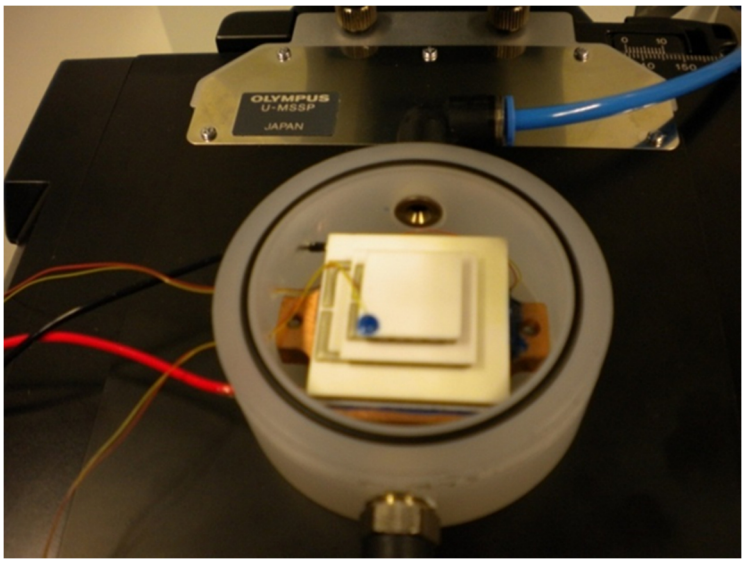

Figure 18 – cryo-cell with thermal-element, Peltier-element and cooling block

Freezing of all samples was done in immersion freezing mode.

Production of Emulsions

Emulsions for cryo-microscopy contained of one part of water and two parts of oil (about 80% of paraffin and about 20% of lanolin). The oil-phase separates the water droplets and simulates the cloud. Generally two methods were used for making of emulsions:

- Two parts of oil and one part of water were pipetted into a test tube which was shaken a couple of times very quickly for several seconds, until the solution turned into milky white which is caused by the Mie-scattering of the water droplets suspended in the oil matrix. Before sample-taking out of the tube the shaking procedure had to be repeated. With help of a single Eppendorf-tip (Pipettenspitzen, Standard, gelb, VWR Collection) the emulsion was directly distributed onto a small glass plate.
- About two parts of oil and one part of water were pipetted in tiny amounts (2-10µl) directly onto a small glass plate and mixed instantly with the tip.

These glass plates were placed under the microscope for detection. Attention was paid to create monolayers of water droplets in the oil-phase. Only these areas were used for analysing the samples.

Experimental Procedure

The glass plates were placed under the microscope as mentioned above. The closed cryo-cell was flushed with nitrogen through gas in- and outlet every time a new sample was put in to avoid humidity from outside, and the blow-dryer was used without heating to avoid fogging on the outside of the cell. Temperature was controlled as described above by varying of current and cooling the thermal block with an ice-water blend.

With assistance of the camera and the software pictures at certain temperatures during the cooling process were taken, until the whole sample was frozen. This process was repeated at least three times for every sample to get statistical distribution of all frozen droplets and to enable statistical data analysis.

Data Analysis

For data analysis the pictures were compared. Changing in the light scattering (Figure 19) gives information, if one droplet is frozen or not. The number of frozen droplets was determined for every picture.

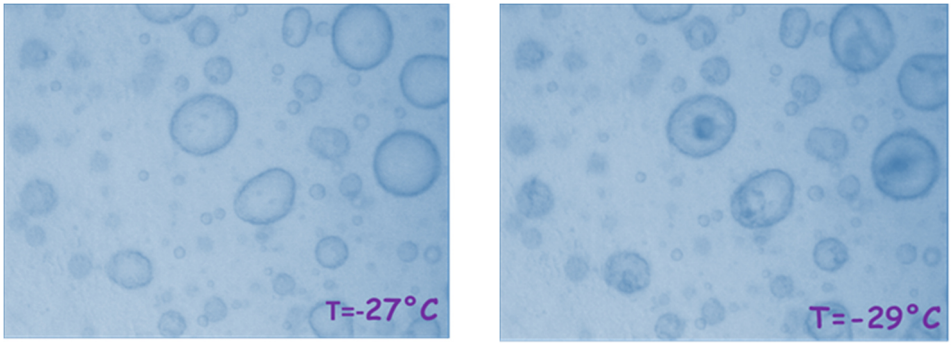

Figure 19 – changes in the scattering of light give information about the frozen drop fraction. Left: sample without any frozen droplets. Right: All droplets are frozen.

The frozen drop fraction for each sample was summed up and depicted in diagrams. Furthermore the median freezing temperature T_{50} was calculated for every sample. This is the temperature where 50% of all droplets are frozen. The temperature in °C was rounded on integer values.

Nucleation rates were determined for selected samples. Emulsions were generated and placed under the microscope as mentioned above and quickly cooled down to a specific temperature which was hold constant over the necessary period of time. Snapshots were taken every second and the frozen drop fraction was plotted against the time. Nucleation rate coefficient were determined for homogeneous nucleation (ultra-pure MilliQ® water) as well as for heterogeneous nucleation (pure plant samples) by using Equation 7 for homogeneous nucleation and Equation 8 for heterogeneous nucleation.

2.4.3 Fourier Transform Infrared Spectroscopy – FTIR

Molecules have three degrees of freedom – translation, vibration and rotation. If an atom consists of n atoms, there are 3n-6 degrees that are motions which change the distance between atoms for non-linear molecules, and 3n-5 degrees for linear molecules, since rotation round the linear axis cannot be observed as an own degree of freedom.

Equation 10 gives the vibrational frequency for a single vibration of a bond.

$$\bar{\nu} = \frac{1}{2\pi}\sqrt{\frac{k}{\mu}}$$

Equation 10

$\bar{\nu}$	Vibrational frequency
k	Force constant of the bond
μ	Reduced mass (ensures that the centre of mass is not influenced by the vibration)

Spectra are defined by the vibrational frequency and depend on masses of atoms, their geometrical arrangement and the strength of their chemical bonds.
Frequency of the mid infrared (IR) light (4000-400cm^{-1}) is in the same range as the vibrational frequency of molecules. Hence infrared radiance can excite molecular vibrations and is absorbed. Infrared spectroscopy can be used to identify molecular structures and compounds. Vibrations that can be observed with IR spectroscopy must be associated with changes in the dipole moment. On the contrary, Raman active vibrations must change polarizability.

Since the 1970ies IR spectroscopy is applied as Fourier transform infrared spectroscopy (FTIR) that offers several advantages. It has three main advantages in comparison to traditional dispersive techniques:

- Throughput or Jacquinot advantage: No monochromator is necessary for FTIR spectroscopy and the amount of light that reaches the detector is not restricted. The throughput is only determined by the diameter of the collimated beam from the source.

- Multiplex or Fellgett advantage: Information from all wavelengths is collected simultaneously which results in a higher signal-to-noise-ratio for a given scan-time and vice-versa.
- Connes advantage: Application of the HeNe-laser leads to higher accuracy of the frequency- or wavelength-axis. Frequency accuracy of 0,001cm^{-1} can be reached.

Figure 20 – Bruker Vector 22 Attenuated Total Reflection FTIR

Figure 20 shows the FTIR spectrometer and the ATR optics that were used for the measurements. ATR enables direct measurement of solid or liquid samples without any pre-treatment. Non-transparent samples can be investigated, KBr mouldings are not needed.

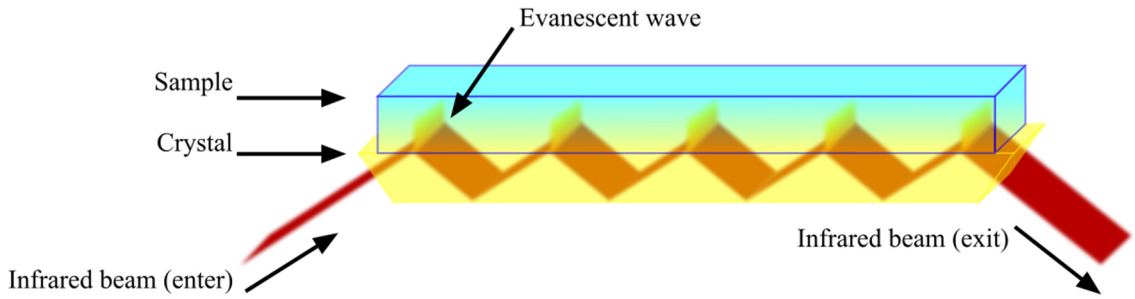

Figure 21 – principle of ATR (source: wikipedia.org)

Figure 21 shows the main principle of ATR-FTIR spectroscopy. The sample is placed on a crystal (Germanium on the used set-up) and the invading IR beam is total reflected in the crystal. When total reflection occurs at the crystal's surface, an evanescent light wave is formed, which decays beyond its surface. The evanescent light wave has a coverage of about one wavelength and might interact with the sample. If the crystal's surface is covered with sample, the total reflected beam loses intensity at wavenumbers, where absorption occurs. ATR-FTIR spectra are not identical to absorption FTIR-spectra, since reflection spectra depend on both the absorption coefficient and the refractive indices. Thus the absorption-reflection bands show different forms due to differences in the ratio between refractive indices and absorption indices of different media.

2.4.4 Residue Determination

Since concentration of the IN of plant samples was unknown, the dry residues of chosen samples were investigated in a pure form. Therefor dry Petri dishes (diameter 55mm, dried under vacuum with desiccator and blue silica gel) were weighted. One millilitre of the chosen sample was pipetted into each Petri dish. These filled dishes were dried under vacuum in a desiccator with blue silica gel for about 48 hours. Afterwards the weight was determined again and the dry residues could be calculated. Evaluation of these data was done by correlation of the frozen drop fraction with the dry weight.

3 Results

Both structural carbohydrates and plant materials were investigated related to their influence on the freezing properties of ultra-pure water. This influence was examined with the already in Chapter 2.4.2 described cryo-microscopy-setup. The used structural carbohydrates can be found in Table 2 and Table 3. Selected structural carbohydrates (chemically modified pectins and altered chemically modified pectins) were additionally investigated by ATR-FTIR (description see Chapter 2.4.3) to see if any altering processes took place. For investigations with cryo-microscopy, aqueous solutions were prepared according to Chapter 2.3.1. Plant materials were used as both juices and extracts (see Chapter 2.3.2). Additionally, DSC-measurements (Chapter 2.4.1) were performed to find a further method for investigations of the influence of different substances on the freezing properties of water.

Freezing curves were established due to the data that were obtained from cryo-microscopy. First the frozen drop fraction was determined (see Chapter 2.4.2).

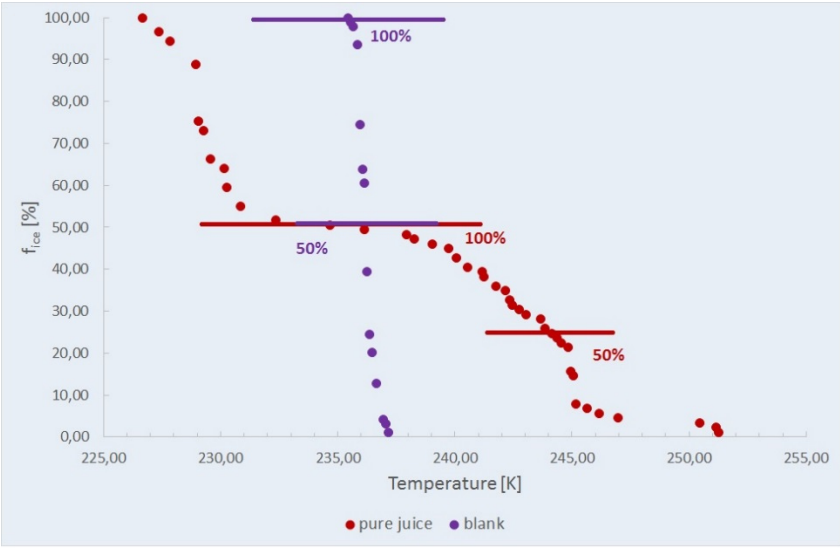

Figure 22 – freezing curve for pure water (one freezing step) and pure chokeberry juice (two freezing steps). Frozen drop factions and T_{50} values were determined. In case of one step freezing curves (blank), the temperature with 50% frozen droplets was determined. In case of two step freezing curves, the first step was set as 100% and the T_{50} value was determined in relation to these 100%.

Figure 22 gives an example for freezing curves (ultra-pure MilliQ water and pure chokeberry juice). On the basis of this figure the information that is obtained from freezing curves shall be explained. As mentioned above, the frozen drop fraction for each temperature is determined. These values are depicted in freezing curves together with the corresponding temperatures. The curves must be read from right to left, beginning with the freezing temperature for the first frozen droplet (first point on the right side near the x-axis of each graph). Due to the decrease of temperature, more droplets freeze. Additionally T_{50}-values were determined (definition see Chapter 2.4.2). In case of one step freezing curves (ultra-pure MilliQ water/blank), this value was directly metered from the curves. In contrast, for freezing curves (chokeberry juice) with two steps, all frozen droplets of the first step were set as 100% and were used as reference for the determination of the T_{50}-value.

3.1 DSC-Measurements

DSC-measurements did not work due to unstable emulsions during freeze/thaw cycles, since the used emulsions showed coalescence during the measurements.

3.2 Carbohydrates

Since carbohydrate polymers are components of all forms of life, they might be an important factor of bio-precipitation, which has already been described in Chapter 1.3 (Figure 10). Carbohydrates that were directly derived from plants and fungi were investigated as well as chemical modifications of both chitin and pectin. A large difference in the influence on the freezing properties of water was found. Alginate, carob gum and the chitin derivatives colloid chitin, chitotriose and chitin resin showed ice nucleation activity in the range between 249K and 241K.

3.2.1 Structural Polysaccharides - Chitin and Chitin Derivatives

Chitin and several chitin derivatives were investigated with cryo-microscopy. An overview over the used samples is given in Table 2, Chapter 2.2.

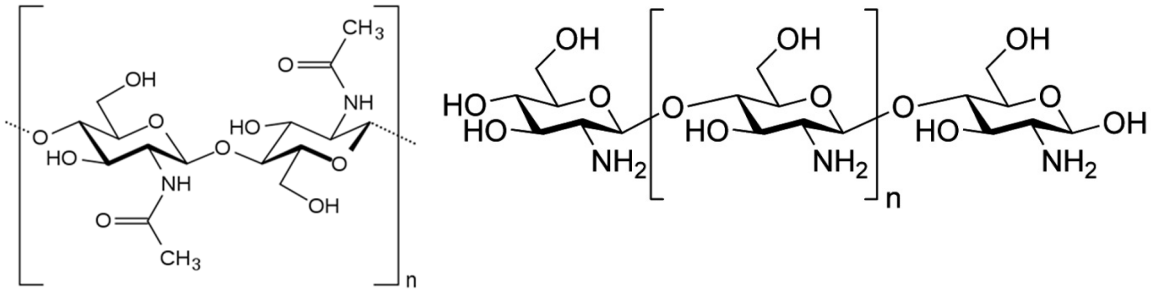

Figure 23 - structure of chitin[13] (N-acetylglucosamine long chain polymer, left) and chitosan[14] (randomly distributed ß-(1-4)-linked D-glucosamine (deacetylated unit) and N-acetyl-D-glucosamine (acetylated unit)) (source: wikipedia.org)

Figure 23 shows the structures of both chitin and chitosan that are components of different forms of life. Chitin is widely spread as structural component in the kingdoms of fungi (cell walls) and animals (exoskeleton of arthropods, mouthpart and structural component of molluscs.). Chitosan (deacylation product of chitin) is contained in the cell wall of some fungi. Chitin shows structural similarity to cellulose which is the structural polysaccharide in plant cell walls. Chitosan has deacetylated side chains, while the side chains of chitin have acetyl groups. All other used chitin derivatives (colloid chitin, chitin

[13] https://en.wikipedia.org/wiki/Chitin#/media/File:Chitin.svg (10.07.2015)
[14] https://en.wikipedia.org/wiki/Chitosan#/media/File:Chitosan_chemical_structural_formula.svg (10.07.2015)

resin and the oligosaccharides chitohexaose and chitotriose) are chemically modified chitin derivatives and do not occur naturally in this form.

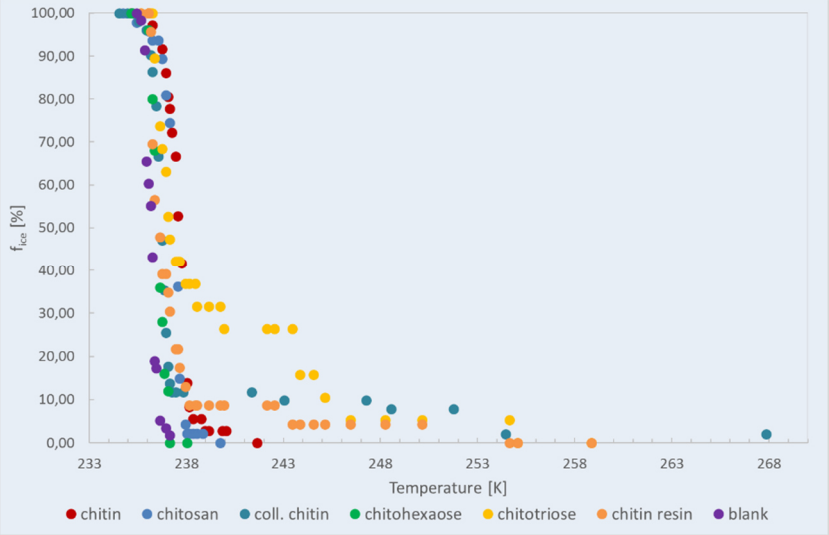

Figure 24 – freezing curves of chitin and chitin derivatives. The freezing curves of chitin (red), chitosan (blue) and chitohexaose (green) are in the same range as the blank, while solutions of chitotriose (yellow), chitinresin (orange) and colloid chitin (blue-green) show freezing curves with more than one step.

Figure 24 shows the freezing properties of aqueous solutions of the chitin derivatives. Sample preparation was done according to Chapter 2.3. It is remarkably that solutions of chitotriose (yellow spots), colloid chitosan (blue-green spots) and chitin resin (orange spots) show freezing properties that differs significantly from the properties of ultra-pure MilliQ water (blank – purple spots). Both homogeneous and heterogeneous IN can be observed in these samples, the freezing curves show two discriminable steps. The first step is in the range of the determined T_{50} values (given in Table 5) and the second step represents the homogeneous nucleation. Latter is in the same region as the blank (purple spots). In case of chitotriose, the first step was assumed as 37% of all droplets since smaller steps were difficult to determine. Unmodified chitin (red spots), chitosan (blue spots) and chitohexaose (green spots) show freezing behaviour very similar to the blank and seem not to have influence on the freezing behaviour of water.

Table 5 – T_{50} values of chitin and chitin derivatives. Values are sorted with decreasing median freezing temperatures.

sample	T50 [K]
coll. chitin	248
chitotriose	244
chitin resin	243
chitin	238
chitosan	237
chitohexaose	236

3.2.2 Water binding Carbohydrates

Investigation of ice nucleation activity of plant substances suggest a detailed view on materials that are used as binding agents since they interact with water in different ways due to their structures and their functional groups. These materials can be derived directly from plants without any modification steps. Several thickening agents and gallants were examined. Artificially altering with ozone treatment was performed for chemically modified pectins. Additional characterisation of both altered and untreated chemically modified chitin samples was done by ATR FTIR spectroscopy. As mentioned above, alginate was the only one water binding carbohydrate that showed clear influence on the freezing properties of water, while the T_{50} value of carob gum [241K] shows a slight, but significant difference to water.

Binding Agents

Guar gum, carob gum, pectin, agar-agar and alginate were investigated on their influence on the freezing properties of water. The chemical structures of these binding agents are depicted in Figure 25.

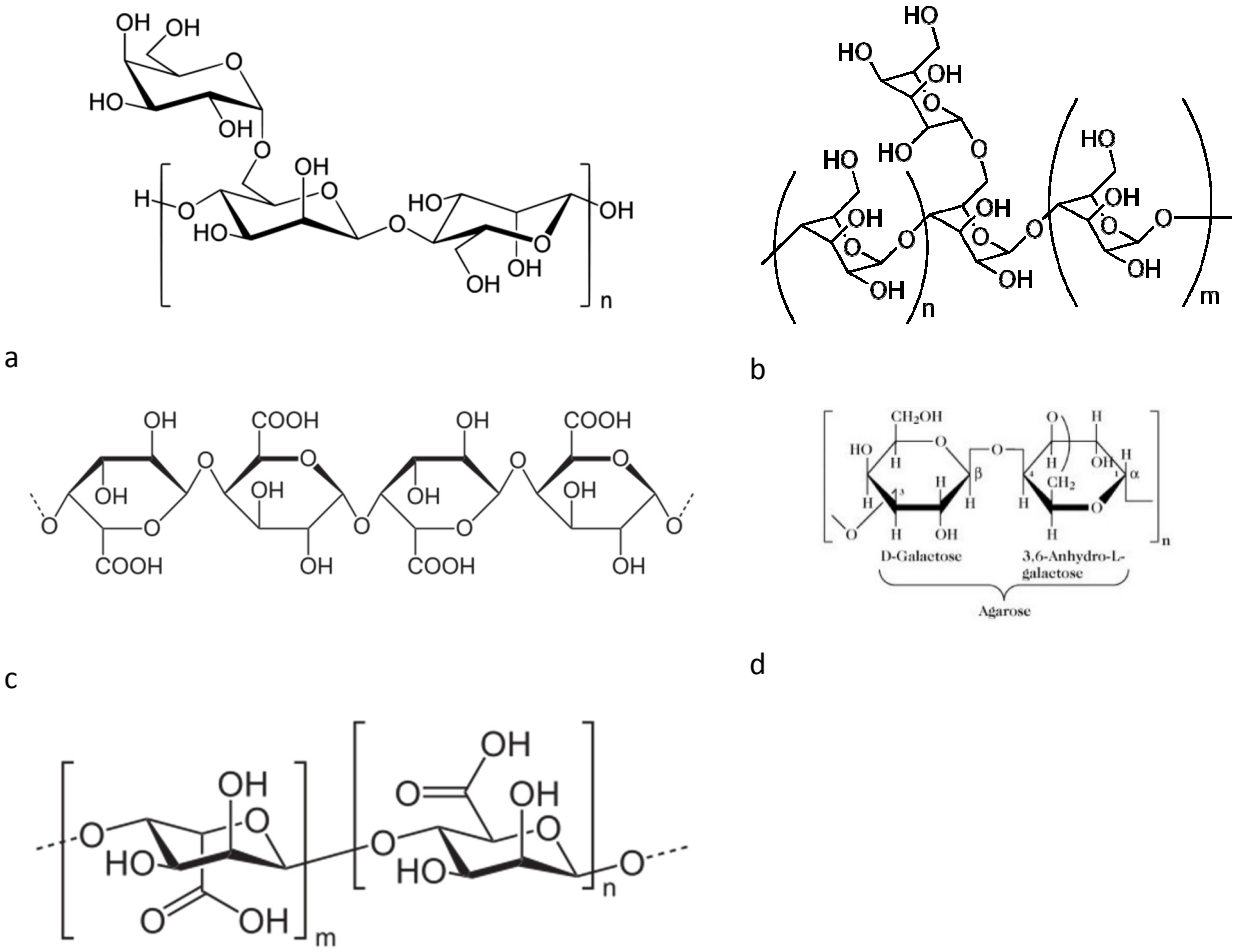

Figure 25 – structures of investigated binding agents. a – guar gum, b – carob gum, c – pectin, d – agar-agar, e – alginate (source: a[15],b[16],c[17],e[18]: wikipedia.org, d: http://www.spektrum.de/lexikon/biochemie/agar-agar/165) (10.7.2015)

Guar gum is a gallactomannan and is obtained from the endosperm of guar beans by dehusking, milling and screening. In foods it is used as thickener and as an additive to ice cream to avoid ice crystal growth. Carob gum, also known as locust bean gum, is similar to guar gum. It is also a gallactomannan, but due to less galactose branch points its solubility and stabilisation-capabilities are lower. Applications are the same as mentioned for guar gum. Pectin is a structural heteropolysaccharide in the primary cell walls of plants. It contains mainly galacturonic acid with different side chains like xylose and arabinose. Pectin is mainly obtained from apple pomace and used as thickener and gelling agent.

[15] https://en.wikipedia.org/wiki/Guar_gum#/media/File:Guaran.svg (10.07.2015)
[16] https://en.wikipedia.org/wiki/Galactomannan#/media/File:Galactomannan.png (10.07.2015)
[17] https://de.wikipedia.org/wiki/Pektine#/media/File:Pektin1.svg (10.07.2015)
[18] https://en.wikipedia.org/wiki/Alginic_acid#/media/File:Algins%C3%A4ure.svg (10.07.2015)

Alginate and agar-agar are both structural polysaccharides in algae. Alginate (also known as alginic acid) is obtained from different brown algae species and consists of guluronate and mannuronate while agar-agar is built up of agarose monomers and agaropectin and is produced by red algae. Both alginate and agar-agar are used for manifold reasons, from food industry over large scale application up to medical purposes.

Saturated solutions were generated by suspending and dissolving the powdery samples in ultra-pure MilliQ water by using the shaking device and the ultrasound bath as already mentioned in Chapter 2.3. These solutions were put into the refrigerator overnight to ensure proper interactions with the added water. Afterward the samples were diluted with water until viscosity was low enough for pipetting. A further dilution step to 1:10 was done and both pure solution and dilution were investigated with cryo-microscopy.

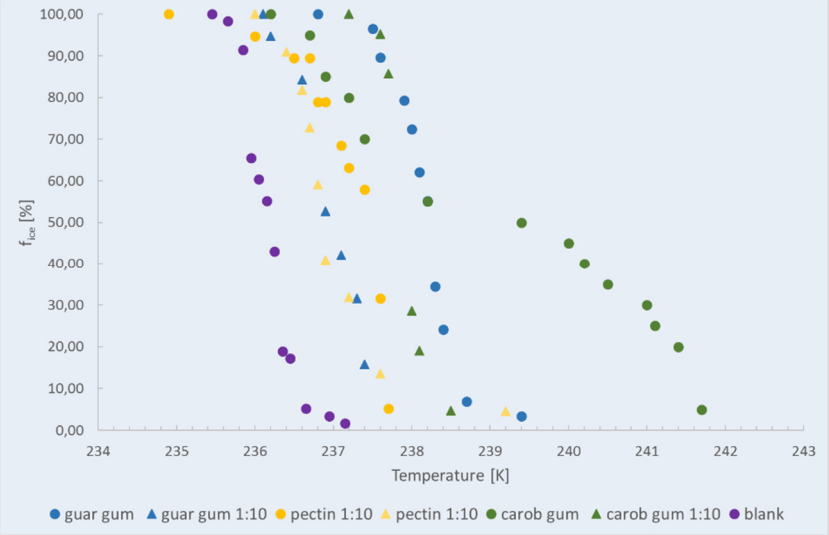

Figure 26 – freezing curves of guar gum (blue), pectin (yellow) and carob gum (green) solutions. Stock solutions are marked as points while freezing curves of 1:10 dilutions are depicted as triangles. Higher concentrated solutions have freezing curves at higher temperature regions. The carob gum solution shows a two-step freezing curves, heterogeneous and homogeneous nucleation can be distinguished.

Figure 26 shows the ice nucleation activity of the guar gum, pectin and carob gum solutions for each two concentrations. All of these samples, except the carob gum, show freezing behaviour which is slightly different from ultrapure MilliQ® water (blank – purple spots). The pure sample of carob gum (green spots) has the highest median freezing temperature. The determined T_{50} values are listed in Table 6. The freezing curve of carob

gum 1:10 dilution shows two steps in the range of 242K to 239K and at about 236K. The other samples show just one step freezing curves at lower temperatures.

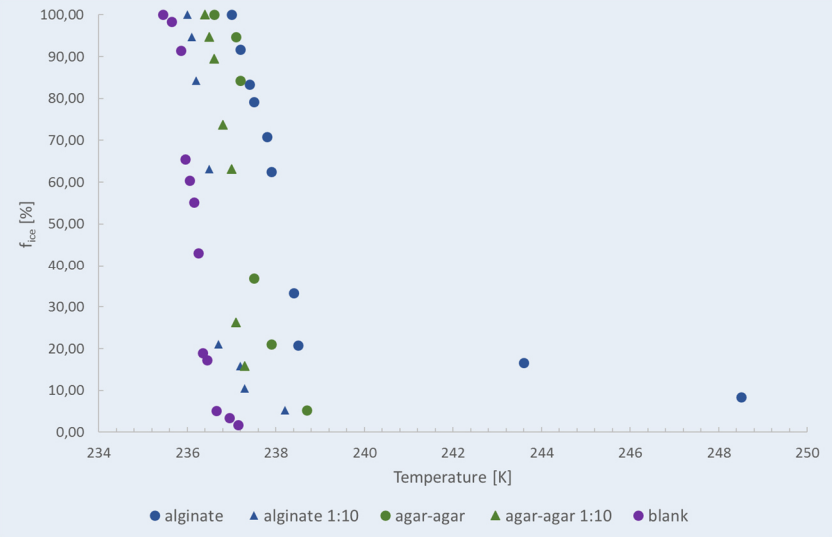

Figure 27 – freezing curves of alginate and agar-agar solutions. All solutions except the agar-agar stock show freezing behaviour in the same range as ultra-pure milliQ water.

Figure 27 shows the freezing curves of agar-agar (green) and alginate solutions (blue). Both solutions of agar-agar and the 1:10 solution of alginate show only slight differences to ultrapure MilliQ® water (blank – purple spots). The freezing behaviour of the stock alginate solution differs clearly from these samples. Two steps can be seen which represent the homogeneous (35%) nucleation at about 249K and the heterogeneous nucleation (65%). All T_{50} values are listed in Table 6.

Table 6 – T_{50}-values of investigated binding agents. Values are sorted with decreasing median freezing temperatures.

Sample	**T_{50} [K]**
alginate	249
carob gum	241
guar gum	238
guar gum 1:10	237
pectin 1:10	237
agar-agar 1:10	237
agar-agar	237
pectin 1:10	236
alginate 1:10	236
carob gum 1:10	235

Apple Pectin Flocculation

Apple pectin that was originally used as dietary supplement was investigated regarding its ice nucleation activity. It consist of airy dark brown flakes with size distribution between 0,5mm^2 and 5mm^2. To ensure homogeneous solutions, these samples were milled before using, as described in Chapter 2.3. The exact denomination is “Apfel-Pektin Flocken Nahrungsergänzungsmittel Karl Minck – Apfelfaser und Apfelpektin zur ballaststoffhaltigen Nahrungsergänzung” from “Pharma Naturheilmittel”. The packing showed several structural aggregates. On the one hand a firm layer was formed on the surface which seemed to be oxidised. Samples from this region are marked as “pectin surface”. Inside of the package, several cluster of flocculation were formed, surrounded by single pectin flakes. These aggregates are marked as “Pectin cluster” while the single flakes are marked as “Pectin centre”. Also preparation of saturated solution was done according to Chapter 2.3. These solutions were diluted 1:10 to see any possibly existing dependencies on concentrations. All samples were investigated with cryo-microscopy.

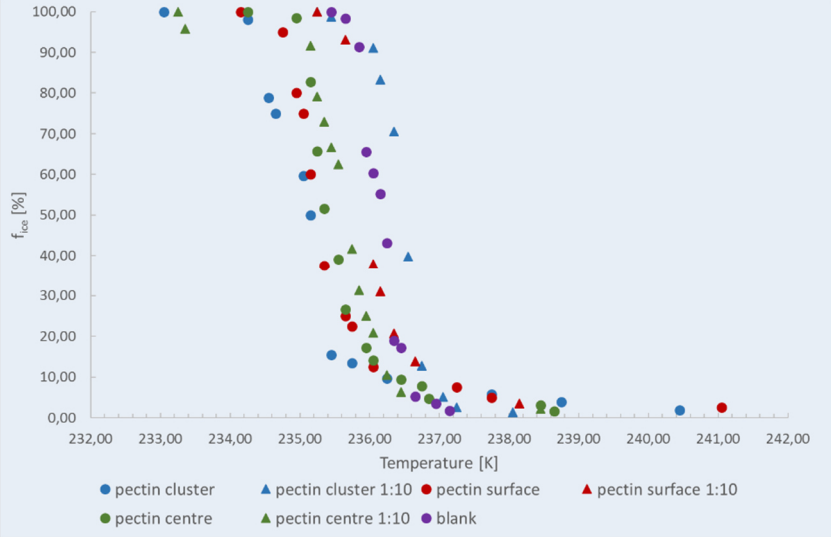

Figure 28 – freezing curves of pectin that was used as dietary supplement. Samples from different points within the stuffing were investigated (clusters inside of the package – blue, samples from the surface – red and samples from the centre of the stuffing – green). Freezing curves of stock solutions are marked as points, while 1:10 dilutions of these solutions are marked as triangles. All freezing curves are in the same range as the blank.

Figure 28 shows the freezing curves of apple pectin. All parts of the above mentioned fractions of the sample show freezing behaviour similar to the blank (purple spots). All determined T_{50} values are in the range between 236K and 235K. Hence conclusions due

to any altering processes inside of the sample cannot be given. Nevertheless preliminary tests that were done with pectin from the surface of the package indicated that there must be some ingredients that influence the freezing behaviour of water. Other preliminary tests showed that pectin from the middle of the package freezes at about 1.5K higher than the other samples.

Chemically modified Pectin and altered chemically modified Pectin

Following samples AU 015, AU 202, AU 601 and AU 701 are chemically modified apple pectins and show differences in the degree of both esterification and amidation, as well as in the content of galacturonic acid. Detailed information about all used chemically modified pectin samples and their chemical properties are given in Table 3.These samples were provided by Fa. Herbstreith & Fox KG. Altering with ozone was done as described in Chapter 2.3 was done. These altered samples were also investigated with cryo-microscopy and are marked as “a” in the following figures. Additional characterisation of these powdery pectin samples was done with ATR-FTIR spectroscopy to see if altering processes occurred. The samples were directly put as powder without any pre-treatment onto the ATR optics. Dry removing of the samples from the optics was done to avoid any moisture, which could be seen in the spectra. Figure 29 gives an overview over the ATR-FTIR characterisation of the chemically modified pectin samples.

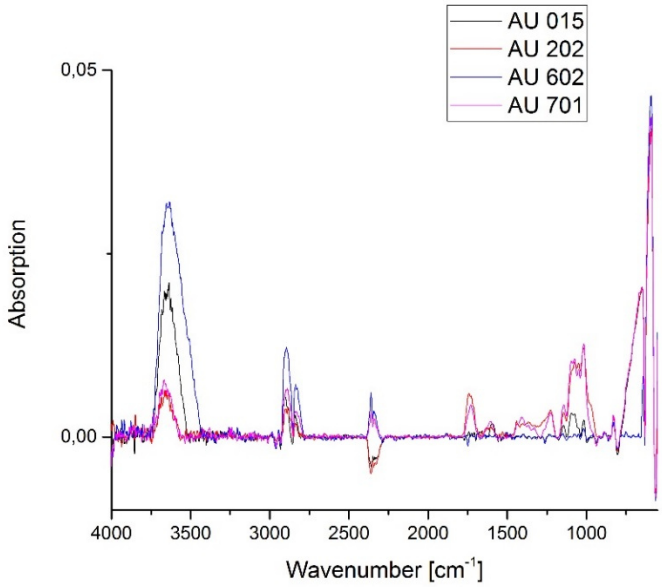

Figure 29 – ATR-FTIR spectra of the used pectin samples without further treatment. Differences between the samples do exist due to their differing chemical modifications. Especially the CO-stretch region shows differences due to both degrees of esterification and content of galacturonic acid.

Peak identification was done in comparison to Synytsya et al., 2003 and is given by Table 7.

Table 7 – peak identification of ATR-FTIR spectra

Wavenumber [cm^{-1}]	**Assignment**
3735-3430	ν(OH)
2935-2860	ν(CH)
2860-2780	ν(CH)
2386-2279	ν(CO_2) due to the ambient air
1770-1680	ν(C=O)$_{COOH}$
1651-1580	$\nu_{as}(COO^-)$

Figure 30 gives a detailed view on the CO-stretch-region between the wavenumbers 2500cm^{-1} and 500cm^{-1}. Due to these curves AU 202 (red) and AU 701 (pink) seem to be more oxidized than AU 015 (black) and AU 602 (blue). They have a higher content of carboxylic acids, ketones, aldehydes and alcohols. Also slight differences between AU 202 and AU 701 exist.

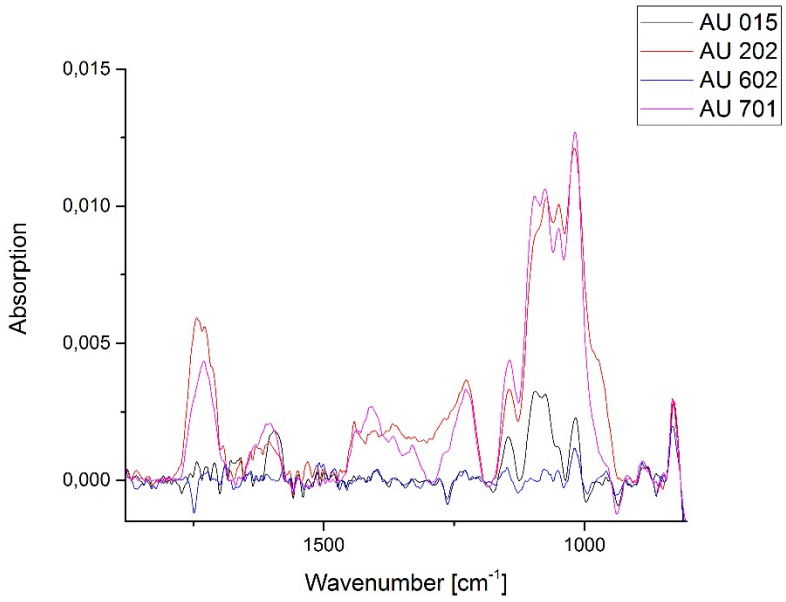

Figure 30 – CO-stretch region of ATR-FTIR spectra between 750 cm^{-1} and 1850 cm^{-1}. AU 202 and AU 701 have higher oxidation states than AU 015 and AU 601. As given in Table 3 AU 202 has the highest amount of galacturonic acid and the highest degree of esterification.

.

Amid AU 015

The detailed composition of Amid AU 015 is given in Table 3, Chapter 2.3. Figure 30 shows the CO-stretch region of the ATR-FTIR spectra of the altered (AU 015a, red spectrum) and the unaltered sample (AU 015, black spectrum). Differences in the CO_2 peaks (not depicted here) are due to the ambient air. The CO-stretch region shows differences between altered and untreated samples. Due to the treatment with ozone, differences in the oxidation states were expected. Especially at wavenumbers between 2000cm^{-1} and 1500cm^{-1} different oxidation states can be observed due to carbonyl stretch bands.

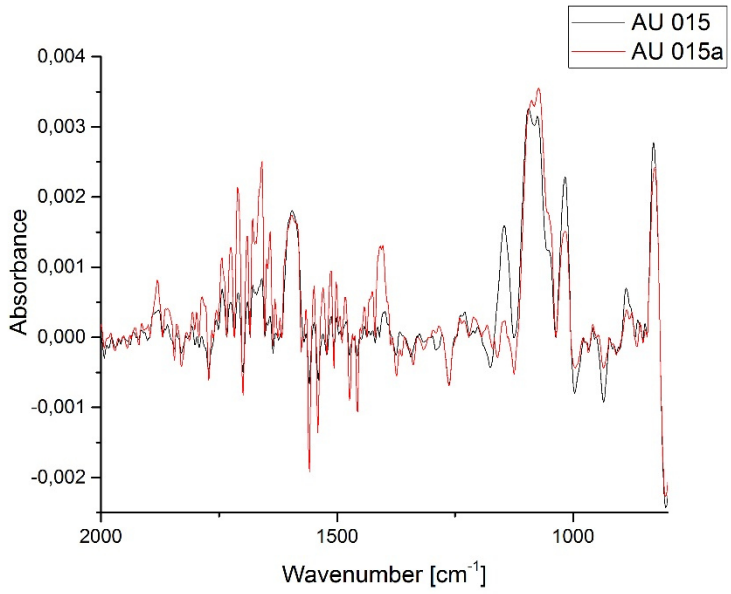

Figure 31 – ATR-FTIR spectra of AU 015 (black) and AU 015a (red) between wavenumbers 2000 cm^{-1} and 800 cm^{-1}. Latter shows higher oxidation states due to treatment with ozone. Bands between 1000cm^{-1} and 1175cm^{-1} might be C-N stretching since AU 015 is amidated. Bands in the region of 1771cm^{-1} and 1635cm^{-1} are due to C=O stretching.

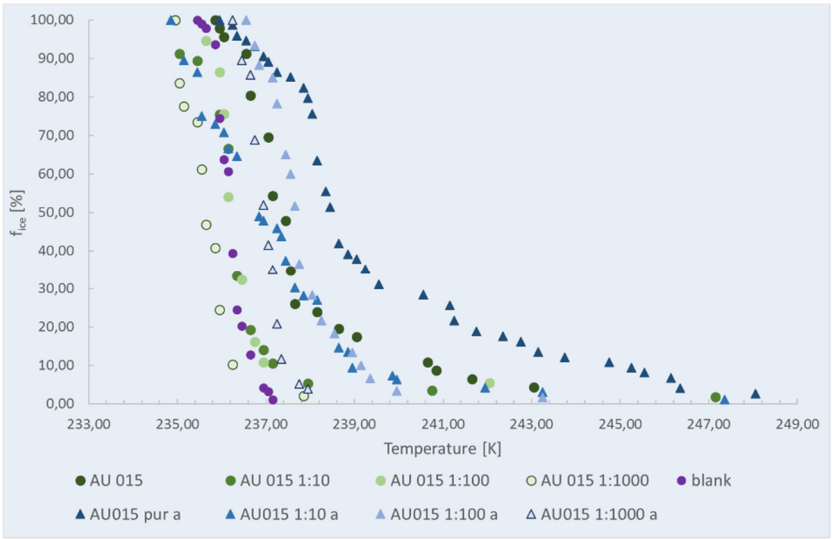

Figure 32 – freezing curves of AU 015 (green spots) and altered AU 015 (blue triangles). The altered sample freezes at higher temperatures. Pure solutions show different freezing properties than diluted samples.

Figure 32 shows the freezing curves of AU 015, marked by blue spots, and altered AU 015, represented by green triangles, in different concentrations. The altered pectin freezes at higher temperatures than the original ones. The pure solution of the altered pectin, has a T_{50} value of 239K, while all other concentrations of both altered and untreated AU 015 freeze in the range of 237-236K. It is remarkable that the freezing curves of highest

concentrations of each sample are significantly different from the other concentrations, which show similar freezing ranges. Determined T_{50} values are given in Table 8.

Table 8 – T_{50} values of AU 015 and altered AU 015 dilutions

Sample	T_{50} [K]
AU015 pur a	239
AU015 1:10 a	237
AU015 1:100 a	237
AU015 1:1000 a	237
AU 015	237
AU 015 1:10	236
AU 015 1:100	236
AU 015 1:1000	236

Classic AU 202

Detailed information about pectin classic AU 202 is given in Table 3, Chapter 2.3. Figure 33 shows the ATR-FTIR spectra of the altered (AU 202a, red) and the unaltered sample (AU 202, black). Differences in the CO_2 peaks are due to the ambient air (not shown in Figure 33). There are differences between the two spectra which might be due to the ozone treatment. These characteristic bands due to C=O and C-O stretching are in the regions between 1892cm^{-1} and 940cm^{-1}.

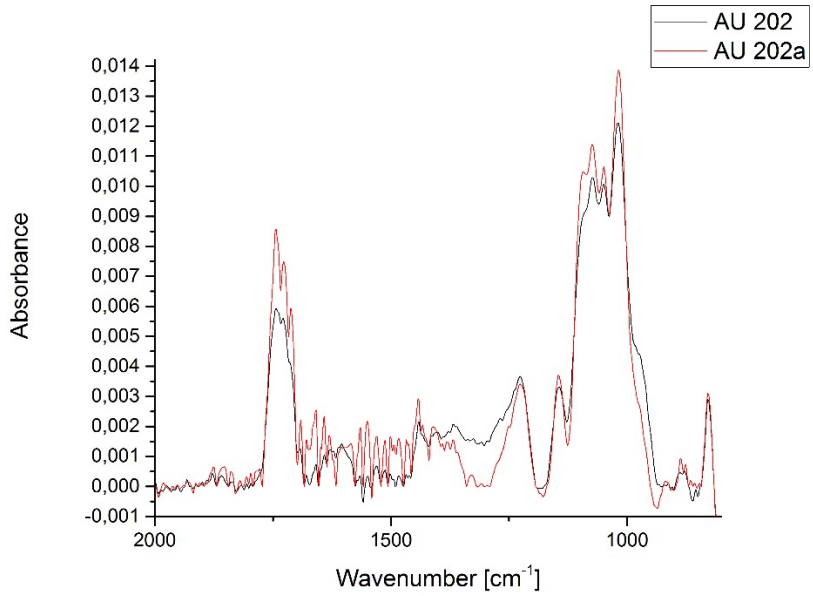

Figure 33 – ATR-FTIR spectra of AU 202 (black spectrum) and AU 202a (red spectrum) between wavenumbers 2000cm^{-1} and 800 cm^{-1}. Latter show higher oxidation states. Due to oxidation processes while ozone

treatment, the red spectrum shows higher intensities between 1890cm^{-1} and 940cm^{-1}. These bands are due to both C=O and C-O stretching.

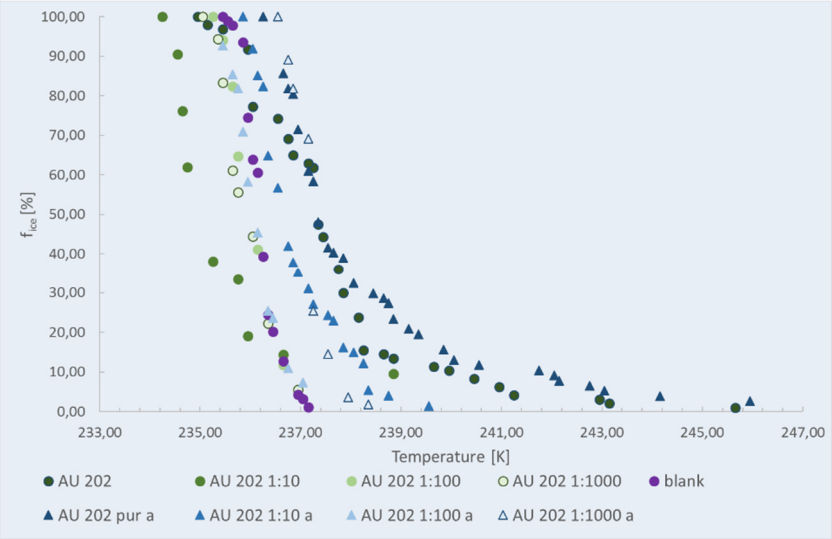

Figure 34 – freezing curves of AU 202 (green spots) and altered AU 202 (blue triangles). The freezing curves of the highest concentration of both samples show similar progresses. The diluted samples of the untreated pectin freeze at slightly lower temperatures than the altered ones.

Figure 34 shows the freezing curves of both pectins AU 202 (spots) and altered AU 202 (triangles) in different concentrations. Several dilutions freeze in the same range (AU 202 in 1:100 and 1:1000 dilution, AU 202a in 1:100 dilution) as the blank (purple spots). The pure samples of both altered and unaltered pectin have the highest freezing temperatures. It is remarkable that the 1:1000 dilution of both samples freezes at higher temperatures than the 1:10 dilution. In all cases, heterogeneous and homogeneous nucleation, if present, cannot be distinguished. The determined T_{50} values are listed in Table 9.

Table 9 – T_{50} values for solutions of both untreated and treated AU 202

Sample	T_{50} [K]
AU 202 pur a	237
AU 202 1:10 a	237
AU 202 1:100 a	236
AU 202 1:1000 a	237
AU 202	237
AU 202 1:10	235
AU 202 1:100	236
AU 202 1:1000	236

Classic AU 602

Detailed information about pectin classic AU 602 is given in Table 3, Chapter 2.3. Figure 35 shows the ATR-FTIR spectra of the altered and the unaltered sample. Due to the spectra oxidation processes must have taken place. The ν(OH) and the ν(CH) are reduced in the altered sample (not shown). The fingerprint region at wavenumbers below 1500cm^{-1} suggests a higher content of oxidised species in the altered sample.

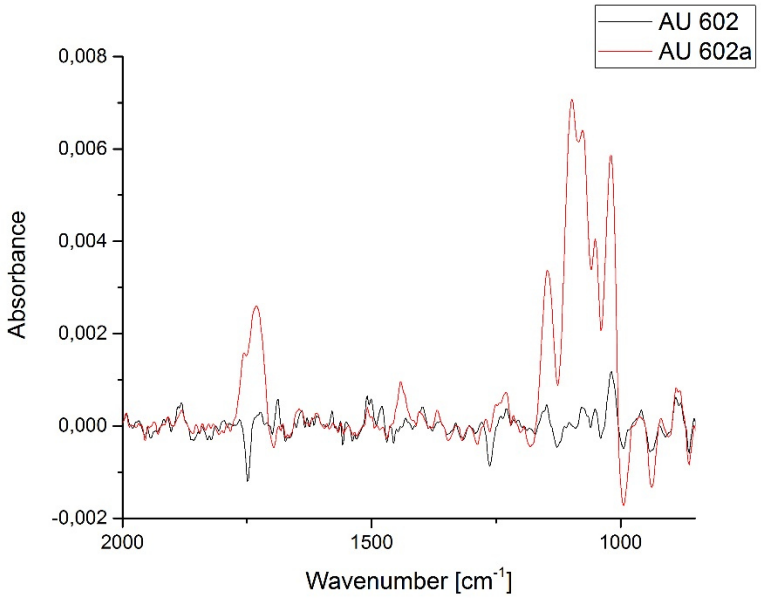

Figure 35 – ATR-FTIR spectra of AU 602 (black) and AU 602a (red) between wavenumbers 2000cm^{-1} and 800 cm^{-1}. Latter has higher oxidation states. Differences between 1250cm^{-1} and 1000cm^{-1} are due to C-O stretching of alcohols and/or carboxylic acids. The band between 1780 cm^{-1} and 1690 cm^{-1} is due to the C=O stretching of carboxylic acids.

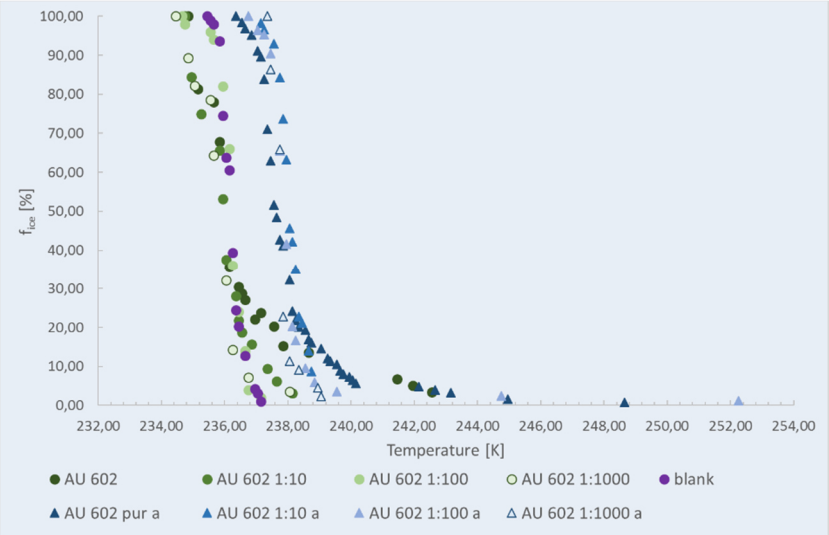

Figure 36 – freezing curves of AU 602 (green spots) and altered AU 602 (blue triangles). The freezing curves of the altered solutions show a slight shift to higher temperatures. No significant differences between the varying concentrations was determined. The untreated sample has freezing curves in the same region as ultra-pure MilliQ water (blank – purple spots).

Figure 36 shows the freezing curves of both altered (triangles) and unaltered (spots) pectin AU 602. The freezing properties of unaltered pectin AU 602 are very similar to the freezing behaviour of ultra-pure MilliQ water (purple spots). The freezing curves of the altered samples are in a tight range and are shifted to slightly higher temperatures. No differences in the freezing behaviour between samples of diverse concentrations could be found. Determined T_{50} values are listed below in Table 10.

Table 10 – T_{50} values of both altered and untreated AU 602 samples

Sample	T_{50} [K]
AU 602 pur a	238
AU 602 1:10 a	238
AU 602 1:100 a	238
AU 602 1:1000 a	238
AU 602	236
AU 602 1:10	236
AU 602 1:100	236
AU 602 1:1000	236

Classic AU 701

Chemical properties of AU 701 are listed in Table 3, Chapter 2.3. Figure 37 shows the ATR-FTIR spectra of the oxidized (red spectrum) and the unoxidized (black spectrum) sample.

Differences in the $\nu(CO_2)$-bands are due to the ambient air (not shown here). Differences in the region between 1775cm^{-1} and 954cm^{-1} are due to oxidation processes while treatment with ozone.

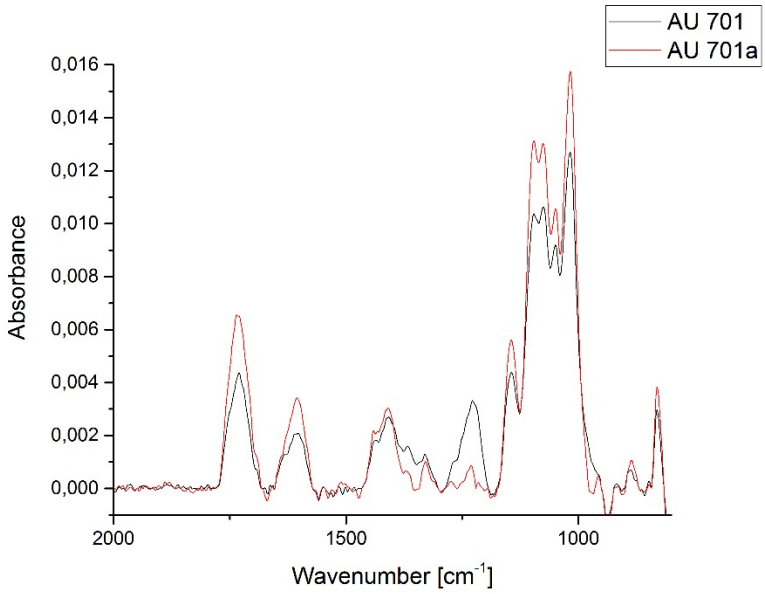

Figure 37 – ATR-FTIR spectra of AU 701 (black) and AU 701a (red) between wavenumbers 2000cm^{-1} and 800cm^{-1}. Differences are due to oxidation processes during the ozone treatment. Bands between 1776cm^{-1} and 1668cm^{-1} might be C=O stretching bands, while bands in the region 1290cm^{-1} to 974cm^{-1} are C-O stretching bands. Hence, there might be an increase of alcohols and carboxylic acids due to altering processes.

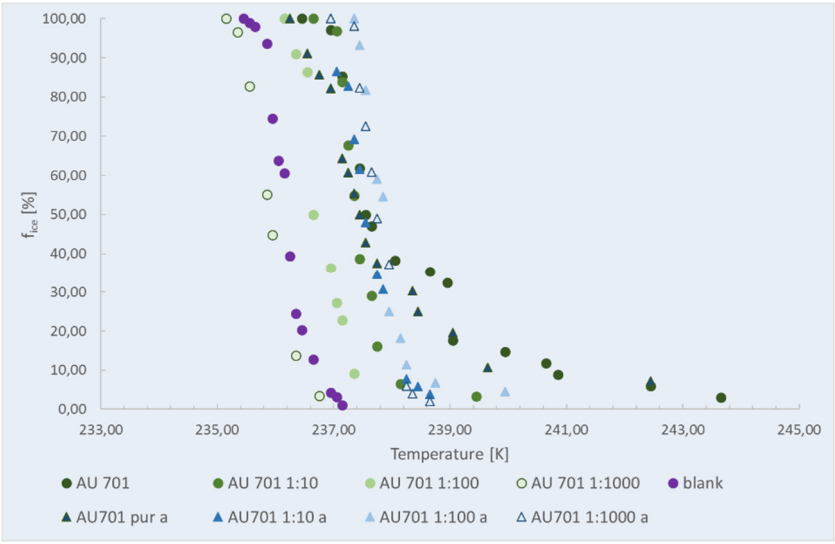

Figure 38 – freezing curves of AU 702 (green spots) and altered AU 702 (blue triangles). Latter samples freeze in closer regions. Freezing curves of both altered and unaltered stock solution are in a similar range. Higher dilution of the unoxidized sample freeze in the region of ultra-pure MilliQ water.

Figure 38 shows the freezing curves of AU 702 (spots) and altered AU 702 (triangles). The altered samples show a tighter freezing range than the unaltered ones. The highest concentrations of both samples show similar freezing curves. The low concentrations of unaltered pectin AU 702 freeze in the same range as the blank (purple spot). Determined T_{50} values are listed in Table 11.

Table 11 – T_{50} values of both altered and unaltered AU 701 samples

sample	T_{50} [K]
AU 701 pur a	237
AU 701 1:10 a	238
AU 701 1:100 a	238
AU 701 1:1000 a	238
AU 701	238
AU 701 1:10	237
AU 701 1:100	237
AU 701 1:1000	236

3.3 Plant Materials

Sample preparation was done according to Chapter 2.3. Also detailed information about the used samples is given in this chapter. All selected samples were investigated by cryo-microscopy. Additionally the dry residues of selected samples were determined to see if there is any correlation between concentrations of IN and the dry residues. Raspberry-juice, cranberry-juice and fenberry-juice were neglected due to the production of tiny amounts (several 100 microliters) in the lab. Also dry residues of plant extract were not determined.

3.3.1 Freezing Curves and T_{50} Values

Bay leaf extract

Bay leaf extract was produced according to the description in Chapter 2.3. It was investigated as additional reference to water since bay leaves do not have their origin at the northern timberline, but are native in the Mediterranean region. Figure 39 shows the freezing curve of bay leaf extract. As expected, the treatment with bay leaves did not have any influence on the freezing properties of ultra-pure MilliQ water, the extract shows the same freezing curve as the blank. T_{50} values of both bay leave extract and water are identical.

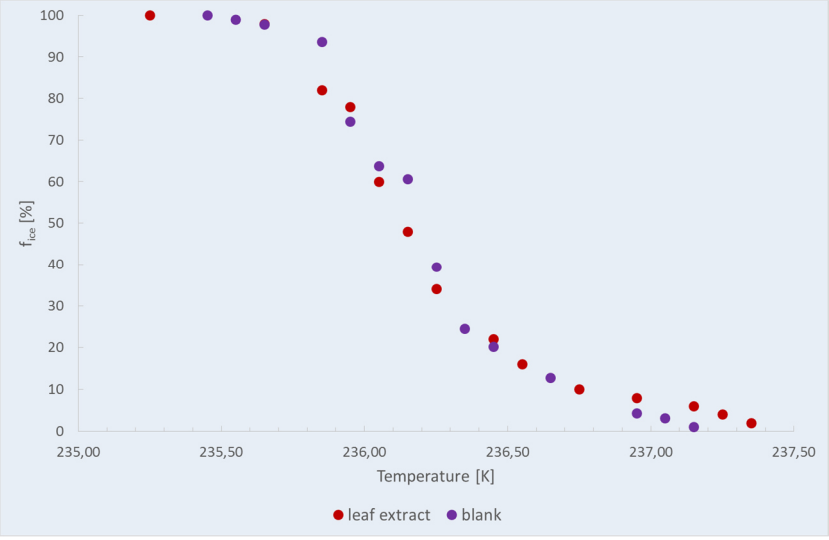

Figure 39 – freezing curve of bay leave (red) extract. There is no differences between the freezing curves of bay leave extract and ultra-pure MilliQ water.

Black Currant

Black currants are small black berries that grow on woody shrubs. They are native in central and north Europe, as well as in northern Asia. The black currant juice sample which was used for the freezing experiments, was bought from "Alnavit". Table 12 gives the dry residues of pure black currant juice and several dilutions.

Table 12 – dry residues of pure black currant juice and several dilutions that were used for cryomicroscopy

Dilution	Concentration [mg/ml]	$f_{ice\ (het)}$ [%]
pure juice	142,9	100
1/10	14,3	100
1/50	2,9	79
1/100	1,4	51
1/200	0,7	34

Figure 12 shows the freezing curve of pure black currant juice and of several dilutions that were determined with cryo-microscopy. Both pure juice and 1:10 dilution show just heterogeneous nucleation. The higher freezing temperatures of the 1:10 dilution are due to freezing point depression by small sugars which are contained in the juice. All other dilutions show heterogeneous as well as homogeneous nucleation in different percentages. It is remarkable that the 1:200 dilutions still contains enough IN for 30% of all droplets.

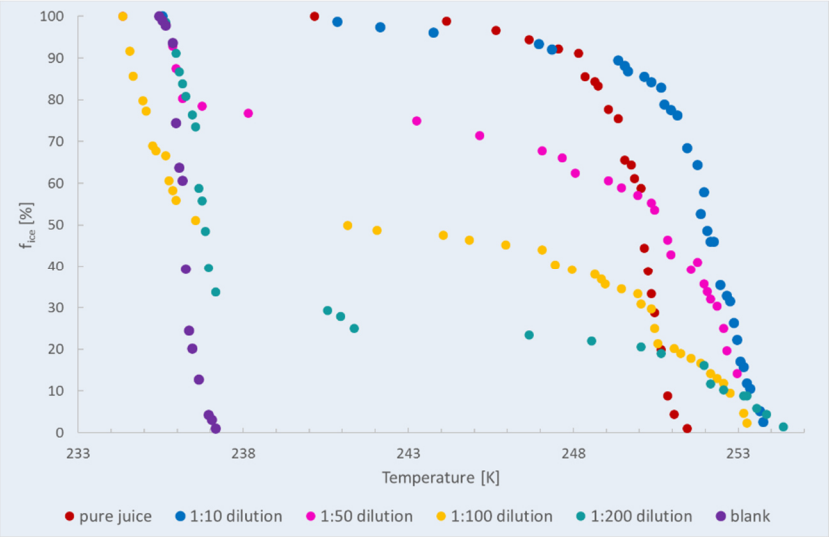

Figure 40 – freezing curves of black currant juice and several dilutions. Pure juice (red) and 1:10 dilution (blue) show only homogeneous nucleation. 1:50 dilution (pink), 1:100 dilution (yellow) and 1:200 dilution (blue-green) have two-step freezing curves.

Determined T_{50} values for all dilutions are listed in Table 13.

Table 13 – T_{50} values of all investigated black currant samples

Sample	T_{50} [K]
pure juice	250
1:10 dilution	252
1:50 dilution	252
1:100 dilution	250
1:200 dilution	251

Blueberry

Blueberries are native widely spread over the northern hemisphere, growing on perennial bushes and trees, reaching heights from several centimetres up to 4 metres. For the investigations of the freezing behaviour directly pressed juice was bought from “Alnavit”. There is no information available which botanical species of blueberries was used for production of juice. Since there were a lot of suspended particles in the juice, one part of it was centrifuged. Table 14 gives the dry residue of the used blueberry juice.

Table 14 – dry residue of the used blueberry juice sample

Dilution	Concentration [mg/ml]	$f_{ice\ (het)}$ [%]
pure juice	119,3	hom

Figure 41 shows the freezing curves of untreated blueberry juice, centrifuged blueberry juice and 1:5 diluted blueberry juice. As the graph shows, there are no significant differences between the centrifuged juice and the untreated juice.

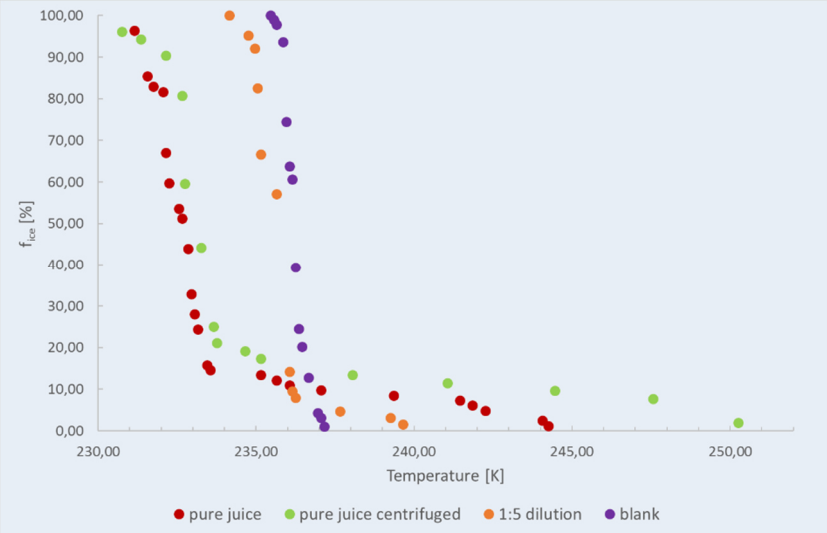

Figure 41 – freezing curves pure blueberry juice (red), centrifuged blueberry juice (green) and 1:5 dilution of pure blueberry juice (orange). All samples freeze at lower temperatures than the blank.

Determined T_{50} values are listed in Table 15.

Table 15 – T_{50} values of investigated blueberry juice samples

sample	T_{50}
pure juice	233
pure juice centrifuged	233
1:5 dilution	236

Chokeberry (Aronia)

Chokeberries are native in eastern North America and grow on bushes, reaching up to two metres. For the investigations of the freezing properties aronia juice from “Alnavit” was used. Table 16 gives the dry residues of the used aronia samples.

Table 16 – dry residues of the used aronia samples

Dilution	Concentration [mg/ml]	$f_{ice\ (het)}$ [%]
pure juice	190,3	48
1/2	95,15	24
1/10	19,03	hom

Figure 42 shows the freezing curves of pure aronia juice, 1:2 dilution and 1:10 dilution. The freezing curve of pure juice shows two steps, representing both heterogeneous nucleation (50%) and homogeneous nucleation (50%). It shows the already mentioned typical flattening of a freezing curve for plant samples. Investigations of the 1:2 dilution showed that about 20% of all droplets got at least one IN, while 80% of the droplets show homogeneous nucleation.

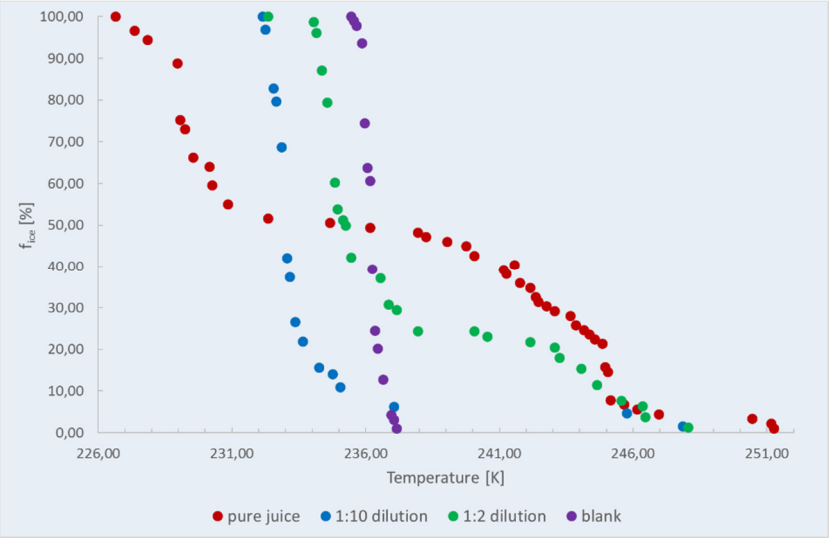

Figure 42 – freezing curves pure chokeberry juice (red), 1:10 dilution (blue) and 1:2 dilution (green). Both pure juice and 1:10 dilution show heterogeneous as well as homogenous nucleation, while the 1:10 dilution is a one-step freezing curve.

Determined T_{50} values of all investigated chokeberry samples are listed in Table 17.

Table 17 – T_{50} values of chokeberry samples

sample	T_{50} [K]
pure juice	244
1:2 dilution	245
1:10 dilution	233

Cloudberry

Cloudberries are small, light pink to light orange berries, growing on small bushes. They have their natural habitats in arctic and alpine tundra as well as in boreal forests. Berries for the investigation of the freezing properties were obtained as frozen berries. Cloudberry juice was produced in the lab by centrifuging the thawed berries for 20 minutes at 3000g in the lab. Figure 43 shows the freezing curves of the berry juice, having lower freezing temperatures than ultra-pure milliQ water. The T_{50} value was determined as 234K, which is below the freezing point of water.

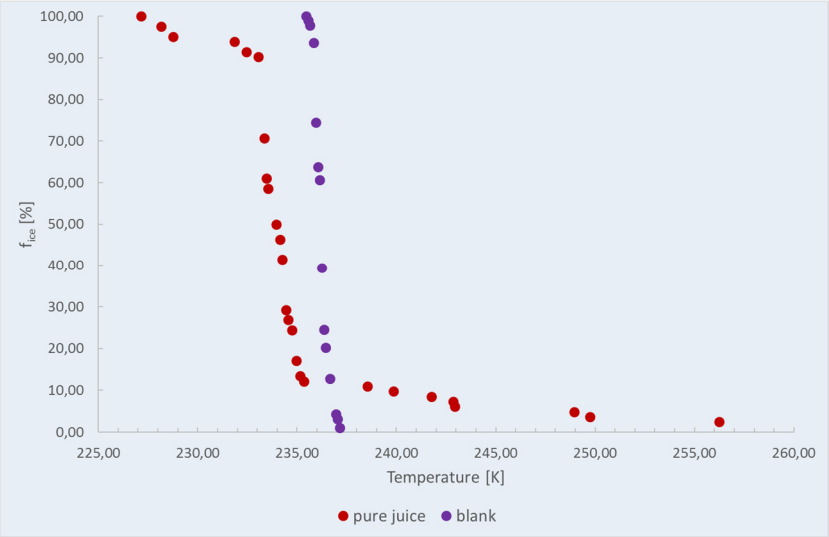

Figure 43 – freezing curve of cloudberry juice (red). No heterogeneous nucleation can be observed.

Cranberry

Cranberries are small red berries growing on low bushes. They are native in North America. The cranberry juice that was investigated with cryo-microscopy was obtained from “Alnavit”. Table 18 gives the dry residues of the used cranberry juice samples.

Table 18 – dry residues of pure cranberry juice and several dilutions

Dilution	**Concentration [mg/ml]**	**$f_{ice\ (het)}$ [%]**
pure juice	99,2	63
1/1	49,6	40
1/5	19,84	23

Figure 44 shows the freezing curve of cranberry juice as well as of two dilutions. The freezing curve of pure juice shows about 60% of heterogeneous nucleation. The typical flattening for plant samples could also be observed. The 1:1 dilution shows that 40% of all droplets did get an IN while 60% of the droplets freeze in the same temperature region as ultra-pure MilliQ water. The 1:5 dilution shows 20% of heterogeneous nucleation and 80% of homogeneous nucleation.

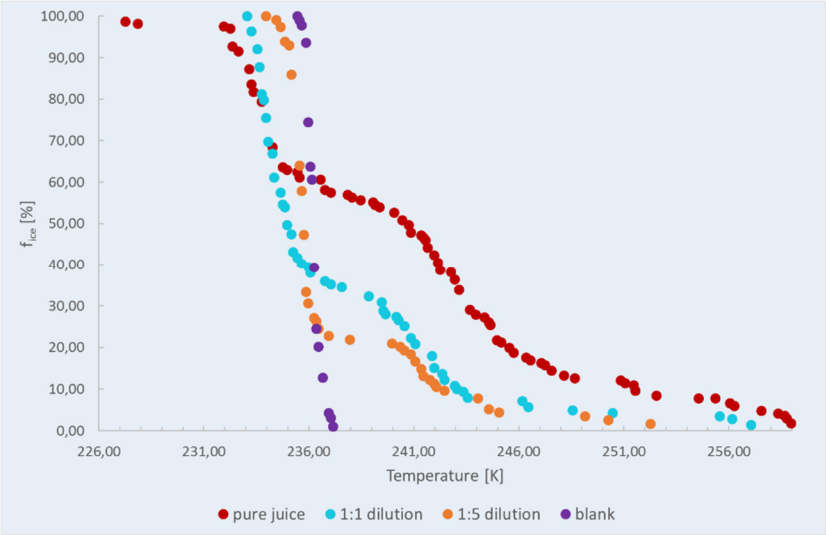

Figure 44 – freezing curve of pure cranberry juice (red) and both 1:1 dilution (light-blue) and 1:5 dilution (orange). All freezing curves are two-step freezing curves.

The determined T_{50} values of cranberry juice samples are given by Table 19.

Table 19 – T_{50} values of cranberry juice samples

sample	T_{50} [K]
pure juice	243
1:5 dilution	242
1:1 dilution	241

Fenberry

Fenberries are small, red berries that grow on low bushes. They are closely relative to both American cranberries and blueberries and have their original habitat in temperate climate in Europe. Berries were obtained as frozen berries and juice was produced in the lab as already described for cloudberries. Again, a fermentation smell could be observed during the thawing process, which might be due to interruptions in the cold chain. Figure 45

shows the freezing curve of fenberry juice. Most of the droplets freeze at lower temperatures than ultra-pure MilliQ water. Due to the spoilage, both freezing curve and T_{50} value (235K) are not significant.

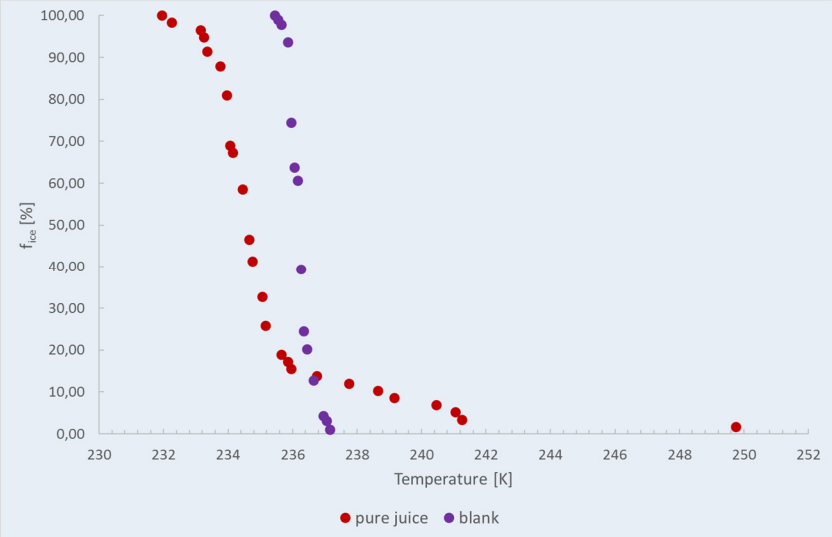

Figure 45 – freezing curve of fenberry juice (red). The curve shows a hint of two freezing steps and a remarkably high initial freezing temperature (temperature where the first droplet freezes). Due to microbial spoilage of the berrys, the curve does have no significance.

Juniper

Juniper is part of the cypress family and widely spread over the northern hemisphere. Its species have their origin from the Arctic to tropical regions in Africa. For investigation of the freezing properties of juniper extract, the extract was produced according to the information in Chapter 2.3. Juniper berries from “Sonnentor” were used for production of the extract. Figure 46 shows the freezing curve of both juniper extract and 1:10 dilution. Nearly all droplets of the pure extract freeze at higher temperatures than the blank. The 1:10 dilution shows the typical flattening for plant samples. About 40% of all droplets show heterogeneous nucleation while 60% of the droplets freeze in the same range as the blank.

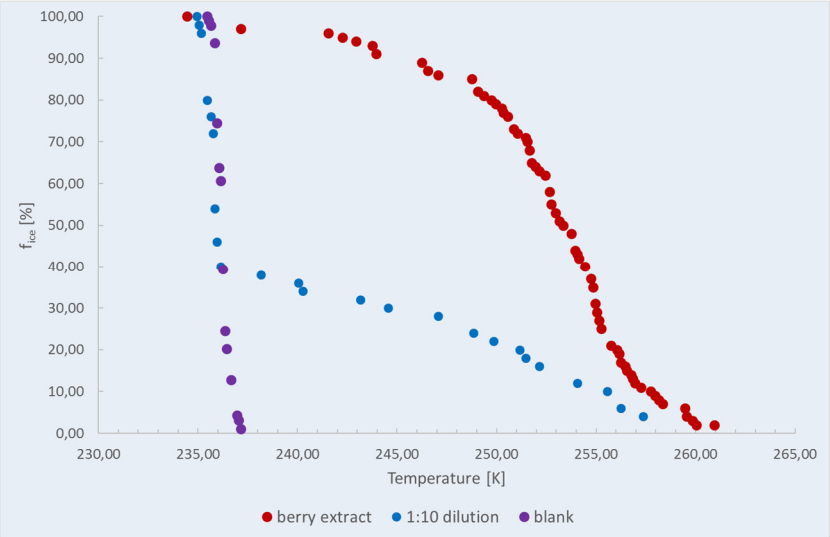

Figure 46 – freezing curve of both juniper berry extract (red) and 1:10 dilution (blue). Nearly all droplets of the pure extract show just heterogeneous nucleation (97%), while 40% of the droplets of the 1:10 dilution freeze at higher temperatures than the blank.

Determined T_{50} values of the juniper berry extract samples are given by Table 20.

Table 20 – T_{50} values of juniper berry extract samples

smaple	**T_{50} [K]**
Juniper berry extract	253
1:10 dilution	251

Lingonberry

Lingonberries are small, red berries, growing on evergreen shrubs. They have their natural habitat in boreal forests and Arctic tundra in the northern hemisphere of Eurasia and are a closely related species to North American cranberries. They are widely spread especially in Scandinavia. Lingonberry juice was obtained as directly pressed juice from “Alnavit”. Table 21 gives the dry residues of the used lingonberry juice samples.

Table 21 – dry residues of both pure lingonberry juice and 1:5 dilution

Dilution	**Concentration [mg/ml]**	**$f_{ice\ (het)}$ [%]**
pure juice	144,3	53
1/5	28,9	40

Figure 47 shows the freezing curve of both pure lingonberry juice and 1:5 dilution. The freezing curve of pure juice might show 2 or 3 freezing steps. It shows a distinctive tendency of flattening that could not be observed in any other sample. About 50% of all observed droplets freeze at higher temperatures than the blank while 20% of the droplets have similar freezing properties as ultra-pure MilliQ water. 30% of all pure juice droplets freeze at lower temperatures than the blank which indicates freezing point depression due to small sugars. The 1:5 dilution shows also an extremely flattening of the freezing curve. Due to the flattening different freezing steps cannot be distinguished. It is remarkable that both freezing curves cross near the blank.

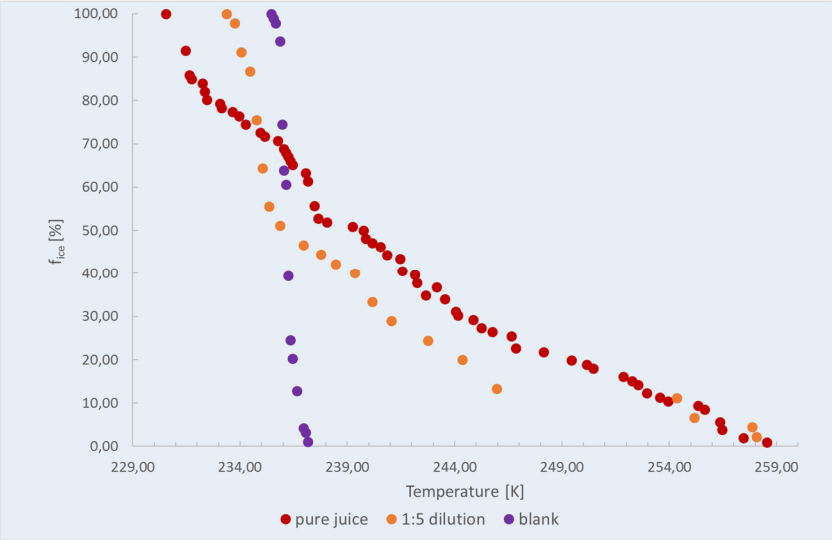

Figure 47 – freezing curves of both lingonberry juice (red) and 1:5 dilution (orange). Due to the steep curves it is difficult to distinguish homogeneous and heterogeneous nucleation.

Determined T_{50} values are given by Table 22. Due to the unusual shape of the freezing curves (no clear discrepancy between freezing curve of pure juice and freezing curve of 1:5 dilution), T_{50} values were difficult to determine.

Table 22 – T_{50} values of investigated lignonberry juice samples

sample	T_{50} [K]
pure juice	247
1:5 dilution	242

Mulberry

Mulberries are 2-3 centimetres long berries, growing on trees in temperate regions all over the world. Mulberry juice was bought as directly pressed juice on the market. No further information about the origin of the used berries and about pasteurization processes could be obtained. Table 23 defines the dry residues of the used samples.

Table 23 – dry residues of mulberry samples

Dilution	Concentration [mg/ml]	$f_{ice\ (het)}$ [%]
pure juice	163,5	100
1/5	32,7	39
1/10	16,4	30

Figure 48 shows the freezing curves of both pure mulberry juice and several dilutions of this juice. The pure juice shows just heterogeneous nucleation. It is remarkable that both 1:5 and 1:10 dilution show very similar freezing properties. There is only a slight difference between these two curves. Both curves show about 40% of heterogeneous and 60% of homogeneous nucleation. Also the typical flattening for plant samples could be observed.

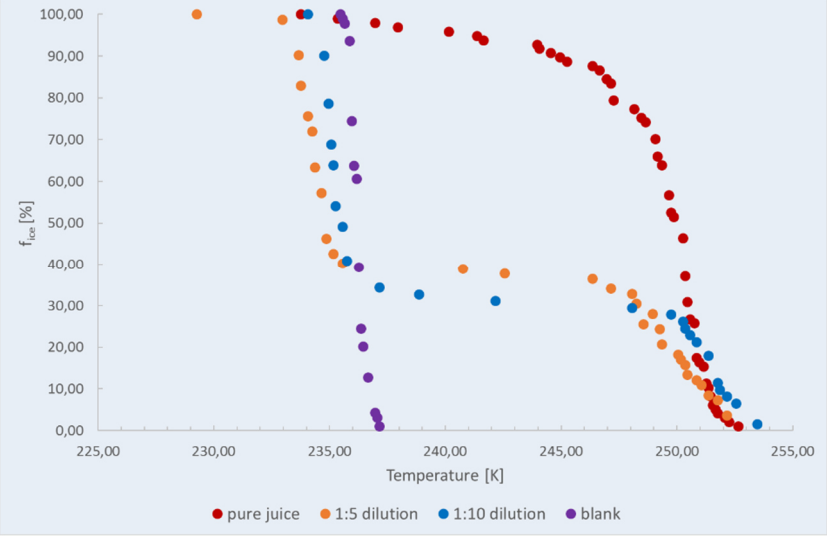

Figure 48 – freezing curves of mulberry juice (red), 1:5 dilution (orange) and 1:10 dilution (blue). The pure juice sample shows only heterogeneous nucleation. The progress of the freezing curves of both 1:5 and 1:10 dilution is very similar. Such slight differences of freezing curves with both homogeneous and heterogeneous nucleation have not been found in any sample.

Determined T_{50} values are given in Table 24.

Table 24 – T_{50} values of investigated mulberry juice samples

sample	T_{50} [K]
pure juice	250
1:10 dilution	251
1:5 dilution	249

Raspberry

Raspberries are small, pink berries that grow on perennial bushes in temperate regions all over the world. There are several commercial cultures that are commercially available. Raspberry juice that was used in this work was produced in the lab by centrifuging thawed, frozen berries that were bought in the supermarket. Figure 49 shows the freezing curves of both raspberry juice and 1:10 dilution. The T_{50} value was determined as 235K.

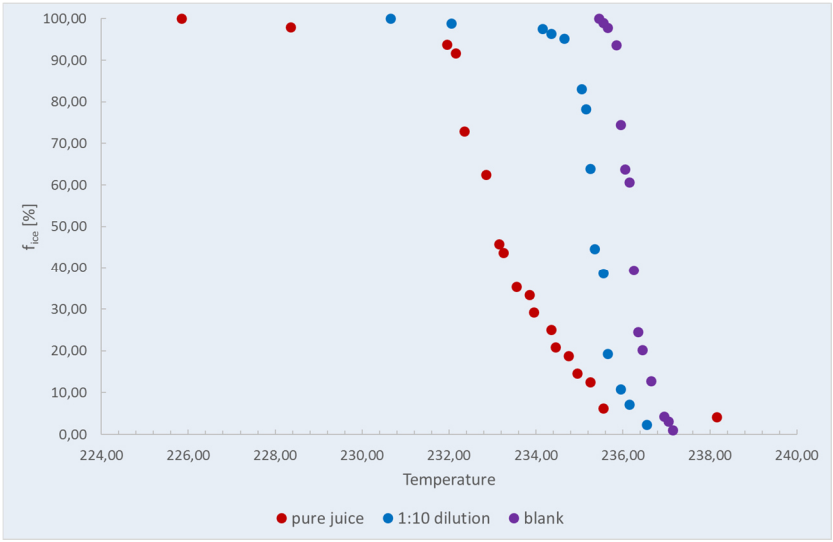

Figure 49 – freezing curves of both pure raspberry juice (red) and 1:10 dilution (blue). Both freezing curves run at lower temperatures than the blank and are one-step freezing curves.

Rowanberry

Rowanberries are small, red berries that grow on 10-15 metres high trees. Due to their high amount of tanning agents they are not used as traditional food. They are widely spread over Europe. The highest occurrence can be found in the foothills of the Alps, as well as in alpine regions and in the Mittelgebirge. Rowanberries were bought as frozen berries, harvested in Styria, Austria. Juice was produced by thawing the berries and using

a household juice extractor, as already mentioned in Chapter 2.3. Additionally the produced juice was centrifuged to get rid of the contained rough particulate matter. Table 25 gives the dry residues of both pure rowanberry juice and 1:10 dilution.

Table 25 – dry residues of both rowanberry juice and 1:10 dilutions

Dilution	Concentration [mg/ml]	$f_{ice\ (het)}$[%]
pure juice	215,8	100
1/10	21,58	29

Figure 50 shows the freezing curves of both pure rowanberry juice and 1:10 dilution. Nearly all droplets of the pure juice show heterogeneous nucleation. The 1:10 dilution shows the already mentioned flattening of plant sample freezing curves. There might be two to three freezing steps which cannot be clearly distinguished because of the flattening. About 30% of these droplets did get an IN, forcing them to freeze at higher temperatures than ultra-pure MilliQ water. 70% of these droplets freeze at lower temperatures than the blank.

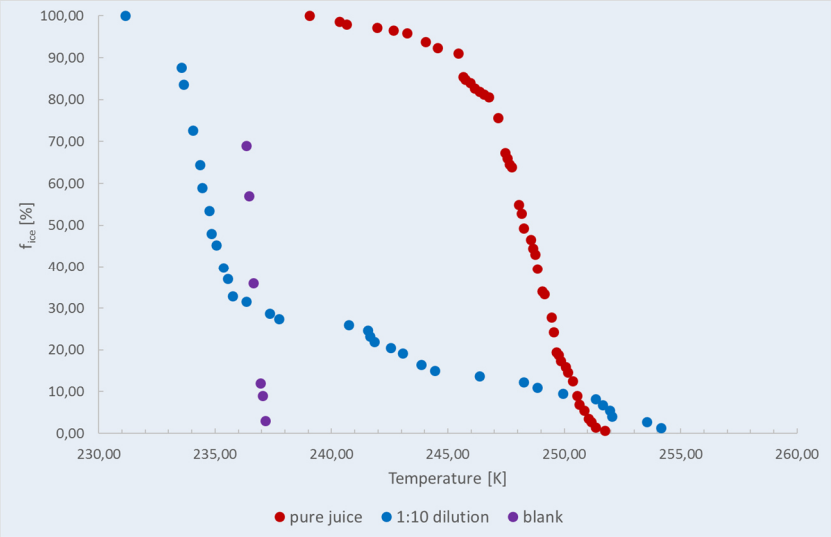

Figure 50 – freezing curves of both rowan berry juice (red) and 1:10 dilution (blue). The pure juice shows just heterogeneous nucleation while the 1:10 dilution has a two-step freezing curve, including both homogeneous and heterogeneous nucleation.

Determined T_{50} values are listed in Table 26.

Table 26 – determined T50 values of investigated rowanberry samples

sample	T_{50} [K]
pure juice	248
1:10 dilution	244

Additionally several extracts of dried rowan berries, bought at a drugstore, and were investigated with cryo-microscopy. Extracts were obtained by putting berries for several days into ultra-pure MilliQ water at room temperature. Due to formation of gas cavities in the tubes, fermentation processes took place. Freezing temperatures of these samples were lower than the blank. The same effects could be observed by investigating samples that were put in the fridge for several days instead of room temperatures. Due to this observations the dried berries seem to be contaminated by yeasts. No further extraction experiments as described in Chapter 2.3 were done.

Sambucus

Sambucus berries are small, nearly black berries growing on small trees or shrubs. They are widely spread over the northern hemisphere and can also be found in Australasia and South America on the southern hemisphere. The used sample was pure juice from "Alnavit". No further information about the geographic origin of this juice was given. Table 27 gives the dry residue of the used sambucus sample.

Table 27 – dry residue of sambucus juice

Dilution	Concentration [mg/ml]	f_{ice} [%]
pure juice	109,5	10

Figure 51 shows the freezing curve of pure sambucus juice. Three freezing steps can be observed. The first step shows heterogeneous nucleation in the range of about 244K, regarding about 10% of all investigated droplets. The second freezing steps occurs in the same region as the blank, containing further 40% of all droplets. The third droplet fraction freezes at significantly lower temperatures than the blank, due to freezing point depression caused by small sugars. For the first step the T_{50} value was determined (245K).

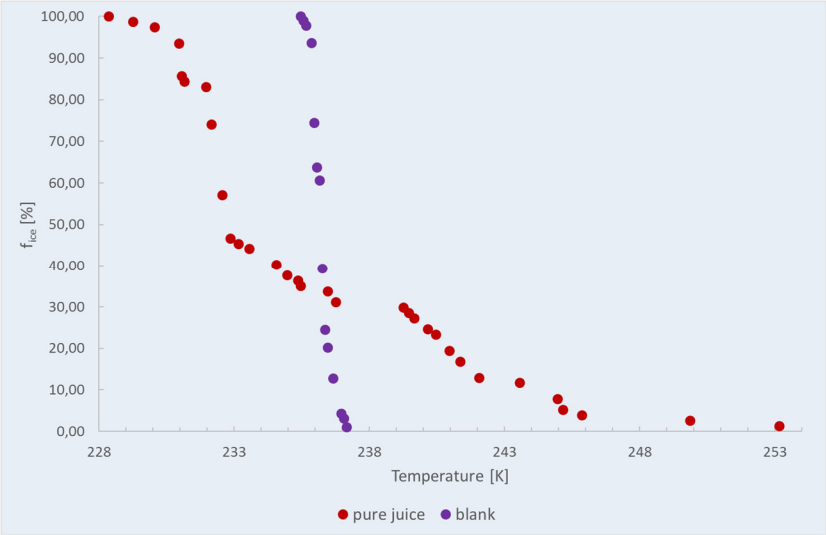

Figure 51 – freezing curve of sambucus juice (red) with three freezing steps. First step represents the heterogeneous nucleation, the second step is in the same region as the blank while the third droplet fraction freezes at lower temperatures than water.

Sea Buckthorn

Sea Buckthorn plants produce small, orange berries and are widely spread over Europe and Asia, as already mentioned in chapter 2.1. Most of the European occurrence can be found at the Northern Atlantic's shore. Sea Buckthorn juice from "Weleda" and "Alnavit" was investigated with cryo-microscopy. The juice from "Weleda" was produced from berries from Tuscany, Italy and pasteurized at about 75°C, while the sample from "Alnavit" was harvested in the Baltic region and Poland, being pasteurized at about 60°C. Both samples were marked as "Muttersaft". No differences in the freezing properties of both samples could be determined with cryo-microscopy. Additionally, centrifuged and uncentrifuged samples were investigated. Again, no differences were observed. Table 28 gives the dry residues of the "Alnavit" sea buckthorn juice samples.

Table 28 – dry residues of the used sea buckthorn samples

Dilution	Concentration [mg/ml]	$f_{ice\ (het)}$ [%]
pure juice	137,8	100
1/10	13,78	70
1/100	1,378	29

Figure 52 shows the freezing curves of pure sea buckthorn juice and of several dilutions. The pure juice shows just heterogeneous nucleation. Both 1:10 and 1:100 dilution show

the already mentioned flattening. 80% of all droplets of the 1:10 dilution did get at least one IN, while 20% of the droplets show homogeneous nucleation. 30% of all droplets of the 1:100 dilution freeze at higher temperatures than the blank, while 70% of these droplets freeze in the same region as ultra-pure MilliQ water.

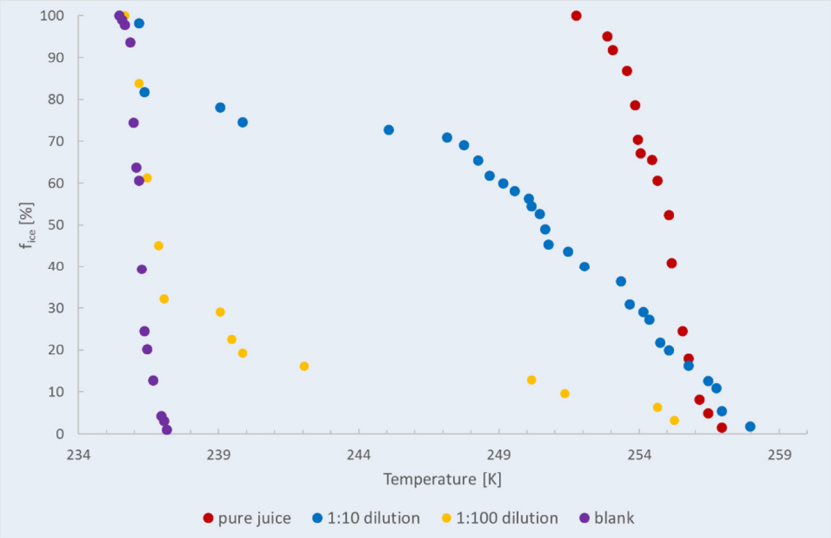

Figure 52 – freezing curves of both pure sea buckthorn juice (red) as well as 1:10 dilution (blue) and 1:100 dilution (yellow). Pure juice freezing curve has one step (heterogeneous nucleation), while both dilutions show two-step freezing curves with homogeneous and heterogeneous nucleation.

The determined T_{50} values are listed in Table 29.

Table 29 – T_{50} values of investigated sea buckthorn juice samples

sample	**T_{50} [K]**
pure juice	255
1:10 dilution	253
1:100 dilution	250

3.3.2 Nucleation Rates

Determination of the nucleation rates was done according to Chapter 2.4.2. Pure juice samples of both sea buckthorn and black currant as well as ultra-pure MilliQ water were used. These two samples were selected due to their high amount of IN. Water was added as a reference to see if results are comparable to literature values. Figure 53 shows the experimental determined nucleation rates. The nucleation rate of ultra-pure MilliQ water is in the same range as it was determined by B. Pummer, 2013. Differences in the grade of the curves are due to singular and stochastic nucleation processes.

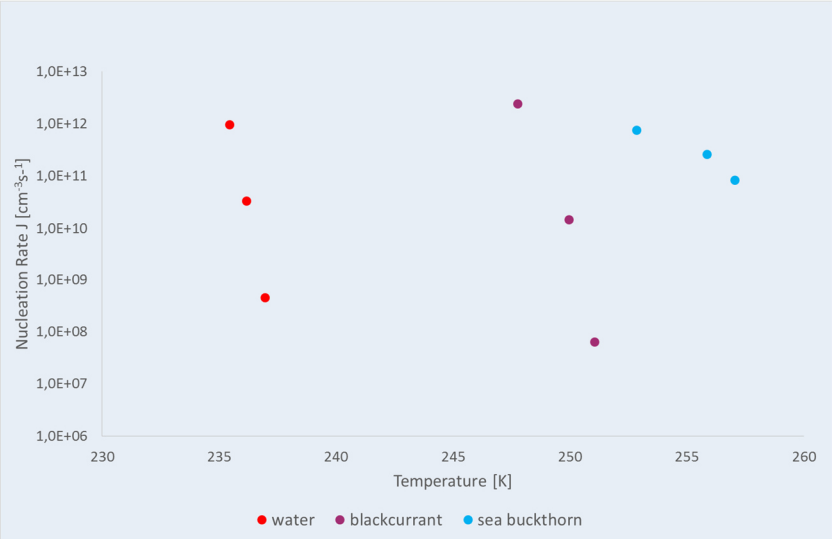

Figure 53 – nucleation rates of ultra-pure MilliQ water (red), pure blackcurrant juice (purple) and pure sea buckthorn juice (blue). The nucleation rate of water can be clearly distinguished from the freezing curves of both juice samples. Blackcurrant juice nucleation rate and the nucleation rate of water show the same rise and show stochastic behaviour, while the nucleation rate of sea buckthorn juice proceeds considerably more plane and can be described by a more singular model.

4 Discussion

Due to the huge amount (33%) of the biologic origin of ice crystal residues (Pratt et al., 2009), further investigations are obvious. Since the 1970ies it is known that some bacteria (Schnell and Vali ,1976; Vali et al., 1976) and other microorganisms (e.g. Kieft and Ruscetti, 1990) contain proteinaceous IN. Furthermore, Pummer et al. (2012) showed that macromolecular IN can be washed off from conifer pollen (e.g. birch pollen). Hence, a broad range of biological material, starting with bacterial fragments and fungi up to parts of both plants and animals are potential sources of IN. Up to now, it is not known if there are any biological IN aside from proteins. In this work both structural and water binding polysaccharides and their chemical modification, as well as some plant materials were investigated due to their ice nucleation activity. Additionally, ATR-FTIR characterisation was done for selected samples of water binding carbohydrates.

4.1 Carbohydrates

Both structural and water-binding carbohydrates were investigated in this research due to their influence on the freezing properties on water.

4.1.1 Structural Carbohydrates

Structural carbohydrates included both chitin and modifications of chitin. Detailed information about the used chitin derivatives is given in Table 2, Chapter 2.3. The determined T_{50} values are depicted in Figure 54. Several modifications of chitin (colloidal chitin, chitotriose and chitin resin) have freezing temperatures with significant differences from the freezing point of water.

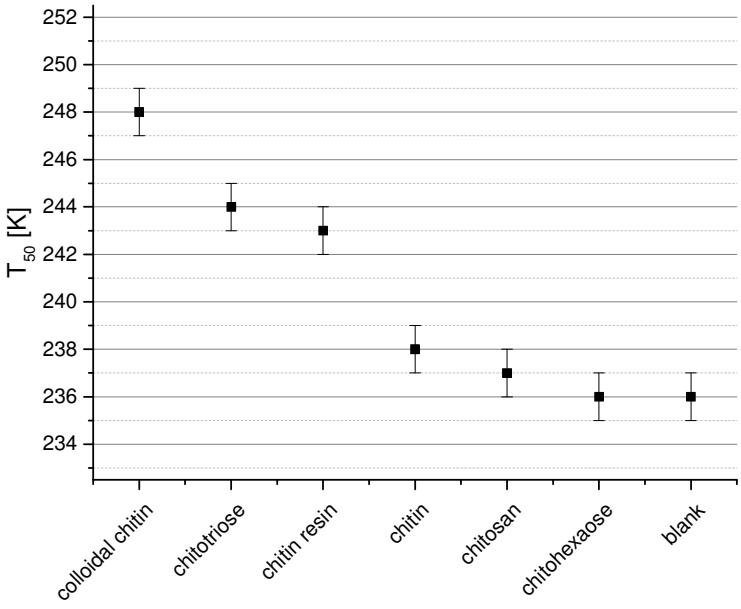

Figure 54 – T_{50} values of all investigated chitin samples. The bars mark the uncertainty of the used experimental setup (±1K). Colloidal chitin, chitotriose and chitin resin show T_{50} values that differ significantly from 236K which is the freezing point of ultra-pure MilliQ water (blank). All these samples are chemically modifications of chitin and are not produced by organisms. All other chitin samples, including both chitin and chitosan that are structural components of many organisms, show freezing behaviour in the range of ultra-pure MilliQ water.

Due to Figure 24 these chitin derivatives have only a small percentage of heterogeneous nucleation. Further investigations with different concentrations of chitin derivatives

would be meaningful, since T. Häusler (2015, private communication[19]) showed that cellulose, which has structural similarity to chitin and which is the structural polysaccharide in plants, influences the freezing properties of ultra-pure MilliQ water in small concentration ranges.

4.1.2 Water binding Carbohydrates

Both gellants and binding agents as well as chemically modified pectin, which are used in food industry, samples were investigated with cryo-microscopy. Due to the already mentioned cellulose experiments (T. Häusler, 2015), binding agents (agar-agar, alginate, guar gum, guar flour and pectin) were investigated in different concentration ranges. It is known that all used samples show very strong interactions with water. It might be possible that water molecules are enclosed by surrounding polymer molecules and fixed this way, being eventually active sites for nucleation processes. The determined T_{50} values of the binding agent samples are depicted in Figure 55. Alginate and carob gum influence the freezing properties of ultra-pure milliQ water significantly.

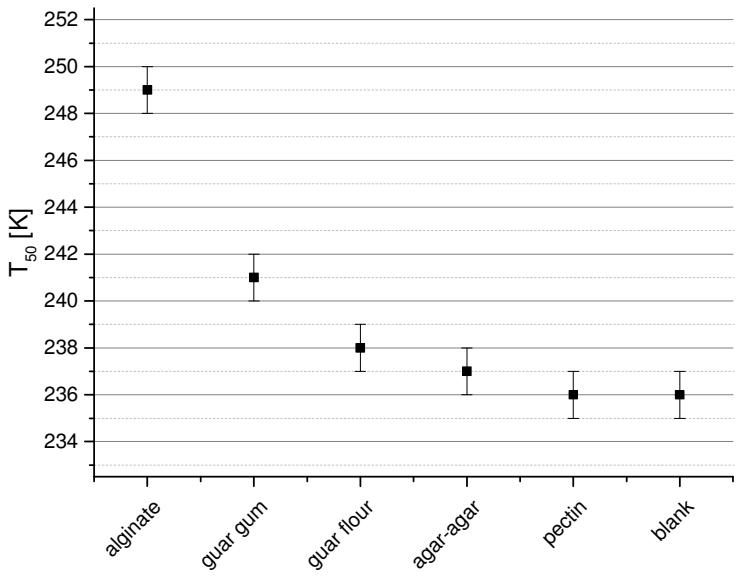

Figure 55 – T_{50} values of all investigated gallants and binding agents. The bars mark the uncertainty of the used experimental setup (±1K). Both alginate and guar gum have significantly influence on the freezing properties of ultra-pure MilliQ water. All other investigated samples (guar flour, agar-agar and pectin) freeze in the same range as water (blank).

[19] Thomas Häusler, TU Wien, Institut für Materialchemie

High concentrations of these samples are difficult to investigate since they build highly viscous solutions, making it hard to generate proper emulsions for cryo-microscopy. In case of managing the preparation of highly viscous emulsions, detection of frozen droplets with analysis of the taken pictures was difficult since there were just slight differences observable concerning the scattering of light. It is feasible that investigations of highly viscous samples would be possible with cryo-DSC. Therefore development of further methods would be necessary. Anyway, alginate is known to release heterogeneous nucleation events. Due to its origin in brown algae it might cause bioprecipitation (see Figure 10, Chapter 1.3) since it is known that marine material can be released by the already mentioned bubble bursting (for detailed information see Chapter 1.3).

The properties of chemically modified pectin samples are similar to results of water interacting polysaccharides. They build highly viscous solutions, causing the already above mentioned experimental difficulties. Altering treatment with ozone were performed for 10 minutes to see if oxidation processes take place. Results of cryo-microscopy (freezing curves are depicted in Chapter 3.2.2, Figure 32 (AU 015), Figure 34 (AU 202), Figure 36 (AU 602) and Figure 38 (AU 701)) and ATR-FTIR measurements (spectra see Chapter 3.2.2, Figure 31 (AU 015), Figure 33 (AU 202), Figure 35 (AU 602) and Figure 37 (AU 701)) suggest that there were marginal distinctive oxidation processes. Since their T_{50} values are close to the freezing point of ultra-pure MilliQ water (Table 8 (AU 015), Table 9 (AU 202), Table 10 (AU 602) and Table 11 (AU 701)), they are not depicted in an extra figure.

4.1.3 Conclusions and Outlook

Due to the T_{50} values of colloidal chitin, chitotriose and chitin resin, as well as to the T_{50} values of alginate and guar gum, one might assume that there are definitively non proteinaceous biological ice nulcei. Nevertheless, there are several further experiments that could be done:

- Concentration-dependent investigations of chitin samples with cryo-microscopy to see if higher concentrations of chitin samples lead to higher percentages of heterogeneous nucleation.

- Ozone treatment for longer time periods could be done for chemically modified pectin samples to see if oxidation processes take place and if there are any influences on the freezing properties of pectin containing water. This oxidation treatment has virtual references since particulate matter that is contained in the atmosphere might undergo oxidation processes due to the presence of ozone. Impacts of ozone to aerosols are due to the residence times and atmospheric heights of the particles.
- Since pectin is contained in many fruits, especially in pomaceous fruits and citrus fruits, it might also be also meaningful doing altering treatment with ozone for both structural and water interacting carbohydrates, since all of them are extracted from several plants and algae and do naturally occur in our environment.
- Also extending of the research to further structural components of plants like lignin or several hemicelluloses would be interesting.

4.2 Plant Materials

Several plant materials from the northern timberline were investigated, primarily berry juices were used since further plant materials like leaves or trunk tissues were not accessible.

4.2.1 Freezing Curves and T_{50} values

Figure 56 shows the T_{50} values of the analysed plant materials.

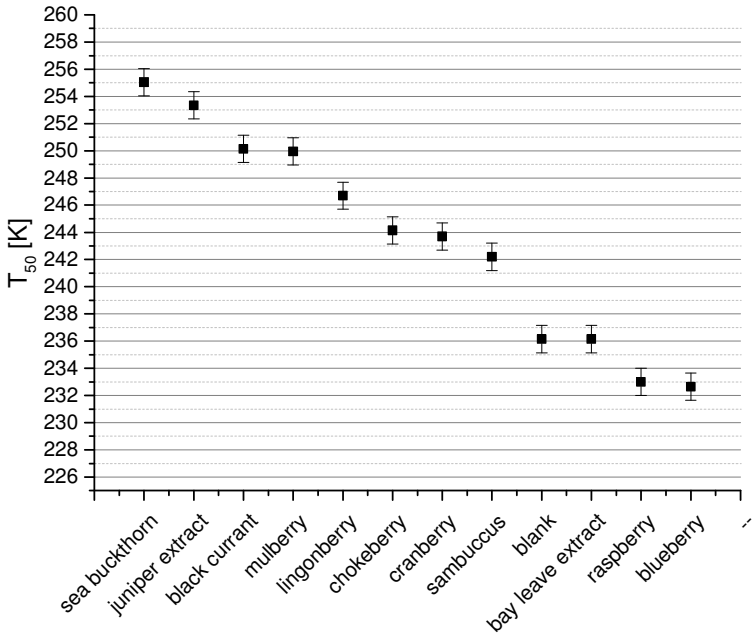

Figure 56 – T_{50} values of all investigated plant samples. The bars mark the uncertainty of the used experimental setup (±1K). Several plant samples, including sea buckthorn juice, juniper extract, black currant juice, mulberry juice, lingonberry juice, chokeberry juice and cranberry juice, freeze at significantly higher temperatures than ultra-pure MilliQ water (blank). Some plant samples have median freezing temperatures below the freezing point of water due to freezing point depression caused by small sugars and salts which are included in every juice sample.

The data of fenberry juice and cloudberry juice are not included since these samples seem to have undergone microbial spoilage, as already mentioned in Chapter 2.3. There are several plant materials that freeze in the range between 255K and 245K. Also birch and juniper pollen have their median freezing temperatures in this range (Pummer et al., 2012). This really tight freezing range suggest a close chemical relationship of the contained IN. It is really remarkable that 7 out of 11 investigated plant samples, neglecting

the obviously spoiled berries, freeze at higher temperatures than ultra-pure MilliQ water. Due to the presence of sugars and salts in all berry juices, freezing point depression occurs. This freezing point depression can also be seen in the freezing curves of black currant juice and its dilutions (Figure 40 - pure juice freezes at lower temperatures than the 1:10 dilution, although both samples show 100% of heterogeneous nucleation), as well as the 1:10 dilution of chokeberry juice (Figure 42), which freezes at lower temperatures than the blank. On principle there are two possibilities for freezing point depression: On the one hand fruit juices contain small sugars and salts that cause freezing point depression. On the other hand, fermentation-smell was observed during the thawing process of cloudberries and fenberries. Due to these facts, the cooling chain of the frozen berries could have been interrupted and freezing point depression could be caused by alcohols. Since all juice samples were pasteurized, latter can be neglected.

It is remarkable that both juniper pollen washing water (Pummer et al., 2012; T_{50}=253K) and extract of juniper berries (T_{50}=250K) have nearly the same T_{50} values. This fact suggests that IN might be present in several plant tissues, not just in berries. Jann et al. (1997) report that IN can be found not just in sea buckthorn berries, but also in leave tissues. Pure sea buckthorn juice has the highest T_{50} value of all investigated plant samples.

Also blueberries do have IN included in their stem tissue, as it was reported in Chapter 2.1. Nevertheless the investigated blueberry juice did not show any ice nucleation activity at all. Even freezing point depression was declared. This might be due to the usage of culture blueberries for juice production. It is rather implausible that wild blueberries were collected and used for juice production. The T_{50} value of raspberry juice might also be due to the usage of culture raspberries for the freezing experiments.

Another interesting fact is the flattening of the freezing curves which could be determined in nearly all freezing curves that show both homogeneous and heterogeneous ice nucleation. Previous investigations in the group showed the same effects for freezing curves of both pollen washing waters and fractionated washing water (Pummer Dissertation, 2013). Also Augustin et al. (2013) determined flattening curves by immersion

freezing of birch pollen washing water. Since Augustin et al. did use another experimental setup (LACIS), the flattening seems not be caused by the used experimental setup. It might be due to slight differences between the active sites of the present IN in plant samples.

Nothing is known up to now about the concentration of the IN in the investigated plant materials. The freezing curves indicate that black currant juice seems to have the highest concentration of IN since the 1:200 dilution shows still about 30% of heterogeneous nucleation. Also sea buckthorn juice does have a remarkable high concentration of IN. The 1:100 dilution has still enough IN for about 30% of all droplets, forcing them to freeze at higher temperatures than water. The IN concentrations of all other investigated plant samples are at least one power of ten smaller than the concentration of pure sea buckthorn juice. No reasons for these facts could be found so far. Dry residues of the berry juices were determined to see whether there is a correlation between the dry residue and the percentage of frozen drops. Figure 57 shows the obtained results.

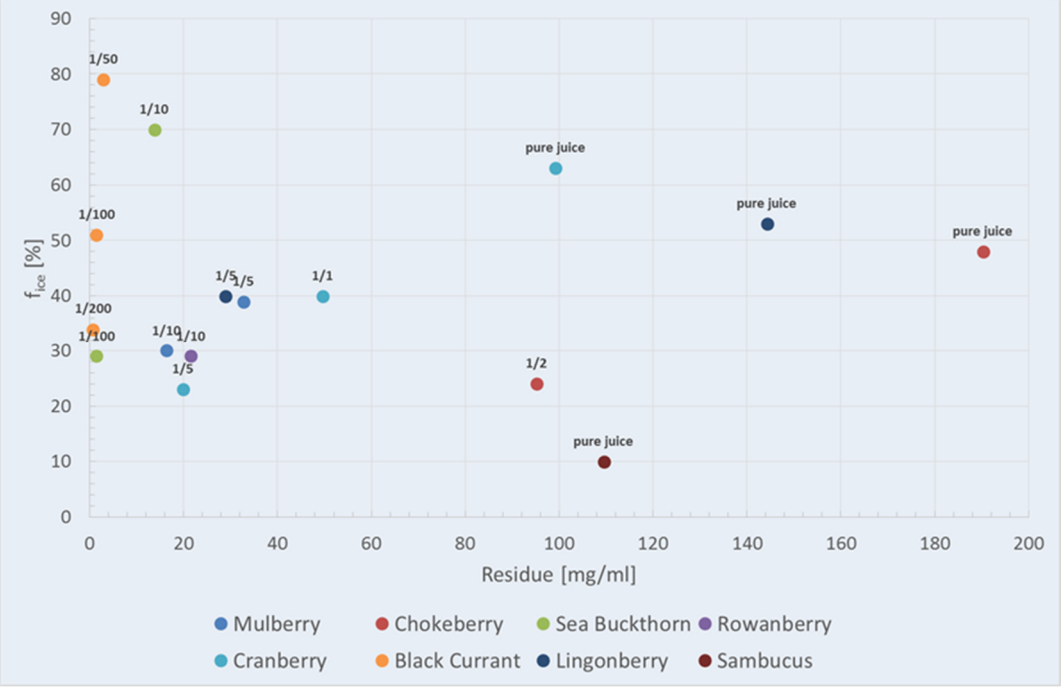

Figure 57 – dry residues related to the fraction of heterogeneous nucleation. Only samples with both homogeneous and heterogeneous nucleation are included. The dilutions of the particular samples are listed above the spots. No correlation between dry residues and the fraction of heterogeneous nucleation could be determined.

Just samples that showed both homogeneous and heterogeneous nucleation were included into this plot. The values are widely spread. Anyway, several regions of concentrations can be distinguished. On the one hand, there is a region with really small amounts of dry residues, representing high dilutions (e.g. 1:100 and 1:200 dilutions). Second region includes 1:10 and 1:5 dilutions, having about 20mg/ml dry residues. Third, there are several samples with really high amounts of dry residues in the right part of the graph. Since the dry residues of mulberries, cranberries, lingonberries and rowanberries are in a tight range, there could be a close botanical relationship between these berries. Additionally correlations within dilutions of the same plant sample can be found. The yellow spots represent the black currant juice dilutions and are within one line. The same effect could be observed for the cranberry sample, the three green-blue spots build a linear slope.

4.2.2 Nucleation Rates

Nucleation rates were determined due to the description in Chapter 2.4.2. Referring to Figure 53, the nucleation rates of ultra-pure MilliQ water and the plant samples can be clearly distinguished. Since pure juice samples were used for determination of the nucleation rates, the bulk of the droplets should contain more than one IN. The exact concentration of IN or active sites is not known up to now. Therefore the nucleation rates could not be confident since one IN per droplet was assumed for determination of the rates. Nevertheless it is interesting that the nucleation rate lines show such different ascending slopes. The nucleation rate of black currant juice has a similar rise as the nucleation rate of ultra-pure MilliQ water. Hence, nucleation processes seem to be similar, meaning that the stochastically model, describing time-dependent nucleation processes, is appropriate for nucleation of black currant juice. In contrast the nucleation rate of sea buckthorn juice shows a much flatter rise, indicating that the nucleation is driven by temperature. This can be described by the so called singular nucleation model. Both singular and stochastic nucleation model are described in more detail in Chapter 1.2.

4.2.3 Conclusions and Outlook

Investigations of the freezing properties of several berry juices and plant extracts show that biological IN are contained in berries from the northern timberline. Due to the presence of IN on birch pollen and the ice nucleation activity of juniper berry extract, there might be also IN in other parts of the plants. Hence, there is potential for further investigations:

- Investigation of wild grown blueberries and raspberries from the northern and/or alpine timberline
- Investigations of non-spoiled fenberries and cloudberries, since they are only native at the northern timberline
- Expanding of the research to further plant materials like leaves, roots or stem-tissue and to non-food plants.
- The size of the IN could be determined by size-exclusion experiments.

5 Literature

Ariya et al., New Directions: The role of bioaerosols in atmospheric chemistry and physics, Atmospheric Environment, 38, 1231-1232, 2004

Ariya et al., Physical and chemical characterization of bioaerosols – Implications for nucleation processes, International Reviews in Physical Chemistry, 28, 1, 1-32, 2009

Augustin et al., Immersion freezing of birch pollen washing water, Atmos. Chem. Phys., 13, 10989–11003, 2013

Becwar et al., Deep Undercooling of Tissue Water and Winter Hardiness Limitations in Timberline Flora, Plant Physiol., 68, 111-114, 1981

Bowers et al., Characterisation of Airborne Microbial Communities at a High-Elevation Site and Their Potential To Act as Atmospheric Ice Nuclei, Applied and Environmental Microbiology, 75, 15, 5121-5130, 2009

Christener et al., Ubiquity of Biological Ice Nucleators in Snowfall, Science, 319, 1214, 2008

Davies and Sykes, Antifreeze Proteins, Current Opinion in Structural Biology, 7, 828-834, 1997

Davies, Ice-binding proteins: a remarkable diversity of structures for stopping and starting ice growth, Trends in Biochemical Sciences, 39, 11, 548-555, 2014

Diehl et al., The ice nucleating ability of pollen Part I: Laboratory studies in deposition and condensation freezing modes, Atmospheric Research, 58, 75-87, 2001

Diehl et al., The ice nucleating ability of pollen Part II: Laboratory studies in immersion and contact freezing modes, Atmospheric Research, 61, 125-133, 2002

Drori et al., Ice-bindig proteins that accumulate of different ice crystal planes produce distinct thermal hysteresis dynamics, Journal of the royal society Interface, 11: 20140526, 2014

Garnham and al., Novel dimeric β-helical model of an ice nucleation active protein with bridged active sites, BMC Structural Biology, 11:36, 2011

Griffith and Yaish, Antifreeze proteins in overwintering plants: a tale of two activities, Trends in Plant Science, 9, 8, 2004

Hansen et al., Formation and annealing of cubic ice: I. Modelling of stacking faults, J. Phys.: Condens. Matter 20, 285104 (12pp), 2008

Huffman et al., Size distributions and temporal variations of biological aerosol particles in the Amazon rainforest characterized by microscopy and real-time UV-APS fluorescence techniques during AMAZE-08, Atmos. Chem. Phys., 12, 11997-12019, 2012

Huffman et al., High concentrations of biological aerosol particles and ice nuclei during and after rain , Atmos. Chem. Phys., 13, 6151–6164, 2013

IPCC, 2013: Climate Change 2013: The Physical Science Basis. Contribution of Working Group I to the Fifth Assessment Report of the Intergovernmental Panel on Climate Change [Stocker, T.F., D. Qin, G.-K. Plattner, M. Tignor, S.K. Allen, J. Boschung, A. Nauels, Y. Xia, V. Bex and P.M. Midgley (eds.)]. Cambridge University Press, Cambridge, United Kingdom and New York, NY, USA, 1535 pp

IPCC, 2014: Climate Change 2014: Synthesis Report. Contribution of Working Groups I, II and III to the Fifth Assessment Report of the Intergovernmental Panel on Climate Change [Core Writing Team, R.K. Pachauri and L.A. Meyer (eds.)]. IPCC, Geneva, Switzerland, 151 pp.

Jann et al., Increasing freezing point of food with sea buckthorn ice nucleating agent, United States Patent 5,665,361, 1997

Jeppsson and Gao, Changes in the contents of kaempherol, quercitin and L-ascorbic acid in sea buckthorn berries during maturation, Agricultural and food science in Finland, Vol. 9, 17-22, 2000

Jia and Davies, Antifreeze proteins: an unusual receptor-ligand interaction, Trends in Biochemical Sciences, 27, 2, 2002

Joly et al., Ice nucleation activity of bacteria isolated from cloud water, Atmospheric Environment, 70, 392-400, 2013

Kajava and Lindow, A Model of the Three-dimensional Structure of Ice Nucleation Proteins, J. Mol. Biol., 232, 709-717, 1993

Kieft and Ruscetti, Characterisation of Biological Ice Nuclei from a Lichen, Journal of Bacteriology, 172, 6, 3519-3523, 1990

Kishimoto et al., High ice nucleation activity located in blueberry stem bark is linked to primary freeze initiation and adaptive freezing behaviour of the bark, AoB PLANTS 6: plu044; doi:10.1093/aobpla/plu044, 2014

Knopf et al., Stimulation of ice nucleation by marine diatoms, Nature Geosciences, 4, 2011

Korolev et al., Microphysical characterisation of mixed-phase clouds, Q. J. R. Meteorol. Soc., 129, 39-65, 2003

Lee, Warren and Gusta, Biological Ice Nucleation and Its Applications, 1995

Lohmann U., A Glaciation Indirect Aerosol Effect Caused by Soot Aerosols; J. Geoph. Res.; Vol. 24 No.4; 11-1 - 11-4; 2002

Lohmann U., Diehl K., Sensitivity Studies of the Importance of Dust Ice Nuclei for the Indirect Aerosol Effect on Stratiform Mixed-Phase Clouds, Journal of the Atmospheric Sciences, 63, 968-982, 2006

Lundheim and Wahlberg, Ice nucleation in fruit juice from different varieties of sea buckthorn *Hippophaë rhamnoides* L., Euphytica, 102, 117-124, 1998

Mak et al., Ice Nucleation induced by *Pseudomonas syringae*, Applied Microbiology, 28, 3, 456-459, 1974

Mishchenko M.I., Rossow W.B., Macke A., Lacis A. A., Sensitivity of Cirrus Cloud Albedo, Bidirectional Reflectance and Optical Thickness Retrieval Accuracy to Ice Particle Shape, J. Geoph. Res., 101, D12; 16973 - 16985; 1996

Möhler et al., Microbiology and atmospheric processes: the role of biological particles in cloud physics, Biogeosciences, 4, 1059-1071, 2007

Morris et al., Bioprecipitation: a feedback cycle linking Earth history, ecosystem dynamics and land use through biological ice nucleators in the atmosphere, Global Change Biology, 20, 341-351, 2014

Murray B. J. and Jensen E.J., Homogeneous nucleation of amorphous solid water particles in the upper mesosphere, Journal of Atmospheric and Solar-Terrestrial Physics 72, 51-61, 2010

Murray et al., Kinetics of the homogeneous freezing of water, Phys. Chem Chem. Phys., 2010, 12, 10380-10387

Murray et al., Heterogeneous freezing of water droplets containing kaolinite particles, Atmos. Chem. Phys., 11, 4191-4207, 2011

Murray et al., Ice nucleation by particles immersed in supercooled cloud droplets, Chem. Soc. Rev., 41, 6519–6554, 2012

Pouleur et al., Ice Nucleation Activity in Fusarium acuminatum and Fusarium avenaceum, Applied and Environmental Microbiology, 58, 9, 2960-2964, 1992

Pratt et al., *In situ* detection of biological particles in cloud ice-cystals, nature geoscience, vol 2, 398-401, 2009

Pummer et al., Suspendable macromolecules are responsible for ice nucleation activity of birch and conifer pollen, Atmos. Chem. Phys., 12, 2541–2550, 2012

Pummer et al., Ice nucleation by water-soluble macromolecules, Atmos. Chem. Phys., 15, 4077-4091, 2015

Pummer, Dissertation, 2013

Pruppacher and Klett, Microphysics of clouds and precipitation, 1997

Sands et al., The association between bacteria and rain and possible resultant meteorological implications, Journal of the Hungarian Meteorological Society, 86, 148-152, 1982

Seidl et al., A complete survey of Trichoderma chitinases reveals three distinct subgroups of family 18 chitinases, FEBS Journal, 272, 5923–5939, 2005

Seinfeld et al., Atmospheric chemistry and physics : from air pollution to climate change, 1998

Schnell and Vali, Biogenic Ice Nuclei: Part I. Terrestrial and Marine Sources, Journal of the Atmospheric Sciences, 33, 1554-1564, 1976

Smolin and Daggett, Formation of Ice-like Water Structures on the Surface of Antifreeze-Proteins, J. Phys. Chem. B, 112, 6193-6202, 2008

Synytsya et al., Fourier transform Raman and infrared spectroscopy of pectins, Carbohydrate Polymers 54, 97-106, 2003

Vali et al., Biogenic Ice Nuclei: Part II: Bacterial Sources, Journal of the Atmospheric Sciences, 33, 1565-1570, 1976

Vali, Interpretation of freezing nucleation experiments: singular and stochastic; sites and surfaces, Atmos. Chem. Phys., 14, 5271-5294, 2014

Wierzbicki et al., Antifreeze Proteins at the Ice/Water Interface: Three Calculated Discriminating Properties for Orientation of Type I Proteins, Biophysical Journal, 93, 1442-1451, 2007

Worrall et al., A Carrot Leucine-Rich-Repeat Protein That Inbibits Ice Recrystallisation, Science, 282, 115-117, 1998